



Politechnika Wroclawska

Doctoral Thesis

**Investigations of Crystalline Lens Wobbling Inertial Motion
Phenomenon by Means of Numerical Simulations**

Author:
Ali Dahaghin

Supervisor:
Damian Siedlecki, PhD

Auxiliary supervisor:
Milad Salimibani, PhD

Ph.D. Programme in **Physics**

October 2024

Abstract

In the research conducted as part of this doctoral dissertation, the dynamic biomechanical behavior of the crystalline lens was analyzed, with particular focus on the oscillation (wobbling) phenomenon taking place immediately after the sudden cessation of the eyeball's rotational movement. Inspired by existing experimental observations, a computational model was developed using the Finite Element Method (FEM) combined with a fluid-structure interaction (FSI) approach to simulate the dynamic phenomena occurring within the eyeball under these conditions. The accuracy of the model was verified by comparing the results of mechanical simulations with experimental data (both *ex vivo* and *in vivo*) obtained from a system for recording Purkinje images and their sequences. This comparison was made possible by using optical simulation software in the computational cycle, which generated Purkinje images analogous to those obtained in experiments. This required a detailed analysis of mechanical parameters. Sensitivity analysis of the biomechanical parameters of individual model structures highlighted the importance of factors such as the Young's modulus of the zonules, on which the lens is suspended, in developing a reliable biomechanical model. Furthermore, the presented research showed that the pressure conditions prevailing in the direct vicinity of the crystalline lens may play a certain role in the dynamics of the lens wobble phenomenon. The results suggest that lens oscillations may in the future serve as a biomarker for non-invasive estimation of intraocular pressure, offering a promising direction for the development of ophthalmic diagnostics. The comprehensive biomechanical approach presented in this work provides a source of new information on the behavior of the lens during rotational eye movements, and the presented results may have implications for both clinical research and the development of diagnostic tools.

Keywords: Crystalline lens, Ocular biomechanics, Fluid-Structure Interaction (FSI), Sensitivity Analysis, Intraocular pressure (IOP)

Streszczenie

W badaniach przeprowadzonych w ramach niniejszej pracy doktorskiej poddano analizie dynamiczne biomechaniczne zachowanie soczewki ocznej, ze szczególnym uwzględnieniem zjawiska oscylacji (kołysania) obserwowanego bezpośrednio po nagłym zatrzymaniu ruchu obrotowego gałki ocznej. Zainspirowany istniejącymi obserwacjami eksperymentalnymi, opracowałem model obliczeniowy wykorzystujący metodę elementów skończonych (FEM) w połączeniu z podejściem oddziaływania płyn-struktura (FSI) w celu symulacji dynamicznych zjawisk zachodzących w obrębie gałki ocznej oku w tych warunkach. Dokładność modelu została zweryfikowana poprzez porównanie wyników symulacji mechanicznych z danymi eksperymentalnymi (zarówno *ex vivo* jak i *in vivo*) pozyskanymi z układu do rejestrowania obrazów Purkinjego oraz ich sekwencji. Porównanie to było możliwe dzięki wykorzystaniu w cyklu obliczeniowym oprogramowania do symulacji optycznych, które generowały obrazy Purkinjego, analogiczne do tych pozyskiwanych w eksperymentach. Wymagało to dokładnej analizy parametrów mechanicznych. Analiza wrażliwości na zmiany parametrów biomechanicznych poszczególnych struktur modelu podkreśliła znaczenie takich czynników, jak moduł Younga więzadełek, na których zawieszona jest soczewka, w opracowaniu wiarygodnego modelu biomechanicznego. Ponadto, zaprezentowane badania pokazały, że warunki ciśnieniowe panujące w bezpośrednim sąsiedztwie soczewki mogą odgrywać pewną rolę w dynamice zjawiska kołysania soczewki. Wyniki sugerują, że drgania soczewki mogą w przyszłości stanowić pewien biomarker do nieinwazyjnego szacowania ciśnienia wewnątrzgałkowego, oferując obiecujący kierunek rozwoju diagnostyki okulistycznej. Zaprezentowane w niniejszej pracy kompleksowe podejście biomechaniczne stanowi źródło nowych informacji na temat zachowania soczewki podczas rotacyjnych ruchów oka, a przedstawione wyniki mogą mieć implikacje zarówno dla badań klinicznych, jak i rozwoju narzędzi diagnostycznych.

Słowa kluczowe: ooczewka oczna, biomechanika oka, interakcja płyn-struktura (FSI), analiza wrażliwości, ciśnienie wewnątrzgałkowe (IOP)

Acknowledgements

I am deeply grateful to my family for their love, support and understanding throughout this challenging but fulfilling journey. Their encouragement has been my source of strength and motivation. Then I would like to express my gratitude to my supervisors, Dr. Damian Siedlecki, Dr. Jorge Grasa and Dr. Milad Salimibani for their support and invaluable guidance throughout my doctoral journey. Their expertise and mentorship have been instrumental in shaping the direction of my research growth. I am also immensely grateful to the host institutions that provided me with the opportunity to conduct research: Wroclaw University of Science and Technology, University of Zaragoza, ARTORG Center for Biomedical Engineering Research, University of Bern, and Johnson & Johnson Surgical Vision (formerly AMO Groningen BV). The resources, facilities, and collaborative environment offered by these institutions have enriched my academic and work experience and facilitated the realization of my research goals. Last but not least, I would like to thank all the individuals who have directly or indirectly contributed to this thesis. Your contributions, whether big or small, have left an indelible mark on this research.

Funding

This PhD thesis was supported by OBERON project funded within the framework of the European Union's Horizon 2020 Research and Innovation Program under the Marie Skłodowska-Curie grant agreement No. 956720 and FEM simulations were carried out using resources provided by Wrocław Center for Networking and Supercomputing (<http://wcss.pl>), grant number 556.

Ethics Statement

This study did not involve any direct *ex vivo* or *in vivo* experiments. Instead, as a reference I used experimental data obtained from previous research conducted by the Visual Optics Group at Wrocław University of Science and Technology, funded by National Science Centre, under the grant agreement No 2019/35/B/ST7/03998.

Related ethics Statements were:

Ex vivo: Ethical approval was not required for the *ex vivo* study involving animals in accordance with the local legislation and institutional requirements because this study used an *ex vivo* porcine eye globe obtained from a local slaughterhouse. Research on this type of sample does not require prior ethical approval according to the law.

In vivo: Informed consent was obtained from the *in vivo* subjects, and the study protocol was in accordance with the guidelines of the Declaration of Helsinki. It was approved by the Bioethics Committee of Wrocław Medical University (application No: 2021/0131).

The data was utilized to develop a finite element method (FEM) model and to reconstruct these experiments *in silico*.

Activities During the PhD Period 2021-2024

Poster and oral presentations:

Dahaghin, A., et al. (2024), "*Effects of intraocular pressure on crystalline lens dynamics.*" Oral presentation at the 12th European Meeting on Visual and Physiological Optics, Wroclaw University of Science and Technology, Poland

Dahaghin, A., et al. (2024), "*Crystalline lens wobbling: In vivo and optomechanical simulation results.*" Poster presented at the 29th Congress of the European Society of Biomechanics (ESB), Edinburgh, Scotland.

Dahaghin, A., et al. (2024), "*Effect of tissue parameters on the dynamics of crystalline lens overshooting.*" Poster presented at the Association for Research in Vision and Ophthalmology (ARVO) meeting, Seattle, Washington, United States.

Dahaghin, A., et al. (2023), "*Investigation of the Crystalline Lens Inertial Overshooting: Ex Vivo and Simulation Results.*" Poster presented at the COMSOL Conference, Munich, Germany.

Dahaghin, A., et al. (2022), "*Ex-vivo Biomechanical Simulations of Crystalline Lens Wobbling in Porcine Eyes.*" Oral presentation at the 10th European Meeting on Visual and Physiological Optics, University of Cambridge, UK

Awards:

Best Poster Award by Popular Vote at the COMSOL Conference, Munich (2023).

Winner of the Hackathon for Grant Writing, University of Antwerp (2023).

Publications:

A. Dahaghin, M. Salimibani, A. Boszczyk, A. Jóźwik, M. Skrok, J. Grasa, and D. Siedlecki. "Investigation of the crystalline lens overshooting: ex-vivo experiment and opto-mechanical simulation results." *Frontiers in Bioengineering and Biotechnology*, 12:1348774, 2024.

A. Boszczyk, F. Dębowy, A. Jóźwik, A. Dahaghin, and D. Siedlecki. "Complexity of crystalline lens wobbling investigated by means of combined mechanical and optical simulations." *Biomedical Optics Express*, 14(6):2465-2477, 2023.

M. Salimibani, A. Dahaghin, A. Boszczyk, J. Grasa, and D. Siedlecki. "Assessment of Material Properties in Key Components of the Porcine Crystalline Lens During Overshooting." *Acta of Bioengineering and Biomechanics*, accepted for publication (30/10/2024).

Submitted Manuscripts:

A. Dahaghin, M. Salimibani, A. Boszczyk, A. Jóźwik, J. Przeździecka-Dołyk, J. Grasa, and D. Siedlecki. "Biomechanical Simulations of Crystalline Lens Oscillations During the Changes in the Gaze in an Accommodated Eye." *Frontiers in Bioengineering and Biotechnology*, date of submission: 1/10/2024.

A. Dahaghin, M. Salimibani, A. Boszczyk, J. Grasa, and D. Siedlecki. "Effect of intraocular pressure on crystalline lens oscillations: a computational study using porcine eye model." *PLOS ONE*, date of submission: 15/5/2024.

Research internships

Three research internships were carried out during the Ph.D. journey:

1. **Institution:** Johnson & Johnson Surgical Vision (formerly AMO Groningen BV), Netherlands.
Supervisor: Dr. Henk Weeber and Dr. Shima Bahramizadeh Sajadi.
Dates: September and October 2024.
2. **Institution:** ARTORG Center for Biomedical Engineering Research, University of Bern, Switzerland.
Supervisors: Ass. Prof. Dr. Philippe Büchler and Dr. Miguel Angel Ariza Gracia.
Dates: February and March 2024
3. **Institution:** Aragón Institute of Engineering Research, University of Zaragoza, Spain.
Supervisor: Prof. Dr. Begoña Calvo Calzada and Ass. Prof. Dr. Jorge Grasa.
Dates: March and April 2023.

Table of Contents

Abstract	i
Streszczenie	ii
Acknowledgements	iii
Funding	iv
Ethics Statement	v
Activities During the PhD Period 2021-2024	vi
Research internships	viii
Chapter 1 General Overview	1
1.1 Thesis Outline.....	2
1.2 Research Hypothesis.....	2
1.3 Research Objectives.....	2
1.4 Structure of the Thesis.....	3
Chapter 2 Introduction	5
2.1 Anatomy of the Human Eye	6
2.1.1 Cornea	6
2.1.2 Sclera	7
2.1.3 Crystalline Lens.....	7
2.1.4 Ciliary Muscles.....	8
2.1.5 Zonular Fibers.....	8
2.1.6 Iris	9
2.1.7 Aqueous Humor.....	9
2.1.8 Vitreous Body	10
2.1.9 Other Structures of the Eye.....	10
2.2 Intraocular Pressure	10
2.3 Crystalline Lens Wobbling.....	11
2.3.1 Experimental Studies.....	11
2.3.2 Purkinje Imaging.....	12
2.3.3 Simple Harmonic Oscillator	15
2.4 Basic Concepts in Eye Biomechanics	15
2.4.1 Finite Element Method.....	16

2.4.2	Mesh Generation.....	17
2.4.3	Mechanical Properties.....	18
2.4.4	Boundary Conditions and Governing Equations	20
2.5	Optics of the Eye	21
2.6	Experimental Inspiration for Biomechanical Simulations.....	23
2.6.1	<i>Ex vivo</i> Experiment	23
2.6.2	<i>In Vivo</i> Experiment	24
	Chapter 3 <i>In silico</i> Reconstruction of <i>Ex vivo</i> Experiment.....	26
3.1	Research highlights.....	27
3.2	Introduction	28
3.3	Materials and Methods.....	28
3.4	Results	31
3.5	Discussion and Conclusions.....	33
	Chapter 4 <i>In silico</i> Evaluation of the Material Effects.....	35
4.1	Research Highlights	36
4.2	Introduction	37
4.3	Sensitivity Analysis	38
4.4	Results	41
4.4.1	Young’s Modulus	41
4.4.2	Poisson’s Ratio.....	45
4.5	Discussion	48
4.6	Conclusion.....	49
	Chapter 5 <i>In silico</i> Evaluation of the Pressure Effects.....	50
5.1	Research Highlights	51
5.2	Introduction	52
5.3	Variation in intraocular pressure.....	53
5.4	Results	55
5.5	Discussion	59
5.6	Conclusion.....	60
	Chapter 6 <i>In silico</i> Reconstruction of <i>In vivo</i> Experiment	61
6.1	Research Highlights	62
6.2	Introduction	63
6.3	Materials and Methods.....	63

6.4	Results	67
6.5	Discussion	71
6.6	Conclusion.....	72
	Chapter 7 Overall Conclusions	73
7.1	Conclusions	74
7.2	Future Research	75
	Bibliography.....	76
	List of Figures	86
	List of Tables	88

Chapter 1

General Overview

1.1 Thesis Outline

When the eye shifts its gaze, it undergoes rapid rotational movement around its center of rotation. Upon abruptly halting this movement, the crystalline lens exhibits motion due to inertia. This phenomenon, known as “wobbling”, likely involves two types of motion: an angular tilt and a lateral displacement of the lens. Despite the apparent influence that intraocular pressure (IOP) might have on these inertial movements, the relationship between IOP and the parameters of lens wobbling has not yet been thoroughly investigated or documented in scientific literature.

The project is meant to have a holistic character, that enables various approaches to study of the lens wobbling phenomenon and detailed investigation of possible relations between its quantitative parameters and the magnitude of intraocular pressure. Numerical methods are used in the project. The choice of porcine eyes is driven by their anatomical similarity to human eyes. The numerical results obtained by means of Finite Element Method modeling of the dynamics and optical simulations of the crystalline lens overshooting performance) will be validated experimentally *ex vivo* and *in vivo*.

1.2 Research Hypothesis

The study supposes that the characteristics of lens oscillatory motion is subject to the ambient conditions inside the eyeglobe. One of these condition is the magnitude of pressure prevailing in the closest neighbourhood of the lens, which is within the anterior and vitreous chambers. Establishing a correlation between the quantitative parameters of the crystalline lens overshooting and intraocular pressure might be of particular importance for advancing IOP measurement methods and development of innovative contactless techniques of IOP estimation. However, before considering the application of lens wobbling as a technique that might be usefull for IOP assessment, or designing a clinical device, a foundational study must be conducted with care to confirm the existence of this relationship.

1.3 Research Objectives

The main goal of this thesis is to understand the nature of the dynamical behaviour of the crystalline lens resulted by rapid changes in the direction of gaze, also referred to as “crystalline lens overshooting”. All specific objectives are the following:

1. Description of the overshooting of the crystalline lens as a phenomenon modeled using Finite Element Method (FEM) simulations. These simulations were developed based on literature data for both porcine and human eyes. The FEM models were used to reconstruct the *ex vivo* (porcine eye) and *in vivo* (human eye) experiments conducted by our research group. This numerical approach allowed for a detailed description of the overshooting, where the lens displacement was characterized as a superposition of both angular tilt and lateral dislocation.
2. Estimate the contribution of the material properties to the characteristics of overshooting.
3. Investigate whether any of the parameters of the crystalline lens overshooting manifest any changes when the average value of IOP is modified.

1.4 Structure of the Thesis

Chapter 2: This chapter introduces ocular biomechanics, emphasizing the eye anatomy of the human eye and its significance beyond vision. It provides an overview of ocular biomechanics, which combines principles from mechanical engineering and physics to analyze dynamic phenomena like the oscillatory motion of the crystalline lens. The chapter also explores various aspects of intraocular pressure, crystalline lens wobbling, and key biomechanical concepts such as the finite element method, mesh generation, and the mechanical properties of ocular tissues. In addition, the chapter highlights how experimental studies serve as an inspiration for biomechanical simulations.

Chapter 3: This chapter discusses crystalline lens overshooting, where the lens shifts excessively after the eye stops rotating. A computational model using finite element analysis was aimed to reconstruct the experimental results.

Chapter 4: This chapter investigates the influence of material properties, specifically Young's modulus and Poisson's ratio, on crystalline lens overshooting. Employing the fluid-structure interaction, it explores different material property scenarios and conducts sensitivity analysis.

Chapter 5: This chapter investigates the impact of intraocular pressure (IOP) on crystalline lens overshooting characteristics by means of FEM simulations under varied IOP levels.

Chapter 6: This chapter serves as the culmination of the present study, determining the potential impact of IOP on human crystalline lens wobbling using an opto-mechanical model.

Chapter 7: This last chapter provides a comprehensive discussion of the findings and unique conclusions drawn from the current study. It also addresses the limitations accompanying this research and, finally, offers valuable recommendations for future research directions.

Chapter 2

Introduction

2.1 Anatomy of the Human Eye

The eye, often considered as nature's masterpiece, epitomizes the marvel of biological engineering. Beyond its role as a mere organ of sight, it embodies a complex interplay of anatomical structures and physiological and optobiomedical processes finely tuned to facilitate vision. The intricacies of its design have fascinated scientists alike for centuries, prompting inquiries into its functional mechanisms. Moreover, recent advances in physiological optics and biomedical engineering have contributed to eye health. From its treatment and potential as a diagnostic tool for systemic diseases, such as Corvis ST (Serbecic et al., 2020, Zhalgas et al., 2019). In this part, I will delve into the anatomy of the eye, exploring its various parts and their functions in detail. In order to ensure a better understanding of the terminology used throughout this study.

In Figure 1 all anatomical components of the eye are shown, but I will focus on explaining the main and most influential parts in terms of biomechanics.

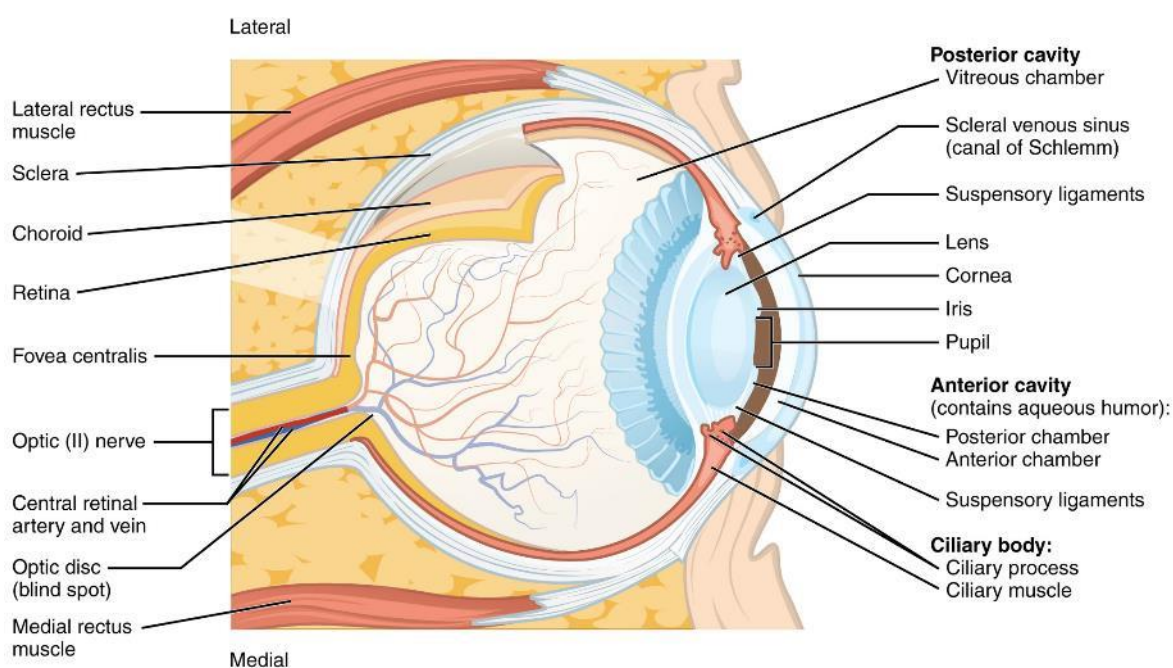


Figure 1. The anatomy of the eye (Betts et al., 2013).

2.1.1 Cornea

The cornea is the clear dome-shaped front structure of the eye that covers the pupil, iris, and anterior chamber. It plays a crucial role in focusing light into the eye. Made up of highly specialized cells and proteins, the cornea is transparent to allow light to pass through easily (Meek and Knupp, 2015) and does not contain any blood vessels. Overall, the transparency,

shape, and sensitivity of the cornea make it a vital component of the eye optical system. It also acts as a protective barrier against dust, germs, and other harmful substances.

The cornea is one of the main components responsible for refracting light as it enters the eye, that is, a curved spherical structure that helps refract light. The ability to refract light onto the inside of the eye is due to that curvature ([Ofri, 2013](#)). The intricate nature of the corneal structure and its crucial role in the visual system has attracted numerous scientists to explore its pathological, physiological, and biomechanical characteristics ([Elsheikh et al., 2007](#), [Piñero and Alcón, 2015](#)). The reason for high sensitivity of any physical interactions on the cornea is due to the presence of large number of nerves. Any damage or irregularities in the cornea can lead to vision problems such as blurred vision, distorted vision, or even vision loss.

2.1.2 Sclera

The sclera is the tough white outer layer of the eye that covers most of its surface. Composed mainly of collagen and elastin fibers, the sclera helps shield the delicate inner structures of the eye from damage ([Watson and Young, 2004](#)), much like the outer shell of an egg. Commonly mentioned to be close to 2.5 times stiffer than the cornea ([Power, 2001](#)). In addition, the sclera serves as a site for attachment of the extraocular muscles, which are responsible for moving the eye in different directions. These muscles, along with the sclera, allow for precise control of eye movements, enabling us to track moving objects and maintain binocular vision.

The sclera remains mostly unchanged during activities that exert mechanical pressure on the eyeball, such as eye movements and rotation, ensuring undisturbed vision ([McBrien et al., 2009](#)). It also plays a role in maintaining the eye's pressure ([Ridley, 1930](#)). The intraocular pressure within the eye is regulated by the balance of aqueous fluid production and drainage. The sclera helps maintain this pressure by providing resistance against the outward expansion of the eye contents. Although the sclera is not directly involved in vision itself, its integrity is essential for overall eye health and function.

2.1.3 Crystalline Lens

The lens system consists of four primary parts: the capsular bag, also known as the capsule, and the crystalline lens, which comprises the cortex and the nucleus. The crystalline lens is a biconvex and transparent structure, positioned behind the pupil within the eye. It plays

a crucial role, often like a camera lens, in the focus of light on the retina, which is essential for clear vision ([Mahil, 2018](#)). The crystalline lens may be small in size, but its significance in the realm of vision cannot be overstated. It has the remarkable ability to change its shape, which in turn adjusts its focal length. This adjustment is crucial for focusing our vision on objects at different distances. This process, known as accommodation, allows us to see clearly objects at near or far distances. This dynamic process is orchestrated by the ciliary muscles, which alter the tension on the zonular fibers, thereby modifying the curvature of the lens ([Wang and Pierscionek, 2019](#), [Beers and Van der Heijde, 1996](#), [Brown, 1973](#)).

The crystalline lens is encased in the lens capsule, a thin, elastic membrane that provides structural support and maintains the shape of the lens ([David et al., 2017](#)). The crystalline lens undergoes continuous changes in shape and flexibility throughout life. With age, the crystalline lens can lose some of its flexibility, leading to a condition called presbyopia, where it becomes harder to focus on close objects ([Heys et al., 2004](#), [Truscott, 2005](#)). Intraocular lenses are synthetic implants used to replace the natural crystalline lens during cataract surgery or refractive lens exchange ([Roszkowska and Torrisi, 2014](#)).

2.1.4 Ciliary Muscles

Ciliary muscles create a ring of smooth muscles located behind the iris of the eye, which surrounds the lens ([Boddu et al., 2013](#)). Within the intricate machinery of the eye, the ciliary muscles stand out as dynamic performers. When the eye shifts its gaze from far to near, the ciliary muscles contract, reducing tension on the zonular fibers and allowing the lens to assume a more rounded shape. This change in shape increases the refractive power of the lens, allowing the eye to focus on nearby objects. Conversely, when the ciliary muscles relax, there is no tension on the zonular fibers, allowing the lens to become thinner and less curved, which is suitable for focusing on distant objects ([Fisher, 1977](#)).

2.1.5 Zonular Fibers

Zonular fibers, also known as zonules or suspensory ligaments, may not be as well known as other components of the eye, but their role in supporting vision is indispensable. They are slender, thread-shaped structures that extend from the ciliary body to the lens of the eye. These fibers serve to suspend the lens within the eye and behind the iris and pupil. This suspension allows the lens to maintain its proper alignment and curvature ([Pan et al., 2023](#), [Streeten, 1982](#)). Their arrangement resembles the spokes of a wheel, radiating outward in a radial pattern.

These fibers play a crucial role in the accommodation process by exerting tension on the lens capsule. Furthermore, zonular fibers possess remarkable elasticity and tensile strength, allowing them to withstand constant fluctuations in intraocular pressure and lens movement during visual tasks ([Wang and Pierscionek, 2019](#), [Bourge et al., 2007](#), [Van Alphen and Graebel, 1991](#)).

2.1.6 Iris

The colored part of the eye, the iris, modifies the pupil's size in order to control the amount of light that passes into the lens ([Napieralski and Rynkiewicz, 2019](#)). This light then reaches the retina, creating an optical image of the surrounding environment. The unique colors of the iris contribute to the aesthetic appearance of the eye, giving each person a distinct look. The iris is composed of two layers of smooth muscle fibers: the dilator pupillae and the sphincter pupillae ([Moazed and Moazed, 2020](#)). In bright conditions, the dilator and sphincter muscles contract, making the pupil smaller to limit the amount of light entering the eye. In dim lighting, they expand, enlarging the pupil to allow more light to enter. The iris and a camera aperture are comparable as a consequence of this characteristic.

2.1.7 Aqueous Humor

The aqueous humor also known as intraocular fluid, is continuously produced inside the eye. It is a watery and transparent liquid that fills the front segment of the eye, between the crystalline lens and cornea. It plays a vital role in maintaining the shape of the eye and providing nutrients, such as glucose and amino acids ([Angayarkanni et al., 2016](#)), to the avascular tissues of the cornea and lens, which do not have direct blood supply. The production and drainage of aqueous humor are tightly regulated processes through specialized channels called the trabecular meshwork and the uveoscleral pathway ([Costagliola et al., 2020](#)).

The aqueous humor also contributes to maintaining the intraocular pressure (IOP) of the eye ([Tamm et al., 2015](#)), which is necessary to maintain the shape of the eyeball and ensuring optimal optical properties and physiological processes. Disturbances in the production, drainage, or composition of aqueous humor can lead to changes in intraocular pressure, which can contribute to conditions such as glaucoma ([Kaufman, 2005](#)), a group of eye diseases characterized by optic nerve damage and vision loss.

2.1.8 Vitreous Body

The vitreous body, also known as the vitreous humor, is a jelly-like substance that fills the space between the retina and the crystalline lens. It is a clear, transparent gel composed mostly of water, along with collagen fibers, and a network of hyaluronic acid molecules ([Kleinberg et al., 2011](#), [Repetto and Tweedy, 2018](#)). The vitreous body helps to maintain the shape of the eyeball and supports the delicate structures within the eye. It acts as a shock absorber, cushioning the internal structures of the eye from sudden movements or impacts. In addition, it plays a role in the transmission of light to the retina, allowing light to pass through to the retina without distortion, and contributes to the overall refractive power of the eye optical system ([Koretz and Handelman, 1988](#)).

2.1.9 Other Structures of the Eye

Retina: A complex layer of neural tissue plays a crucial role in the process of vision by capturing light rays and converting them into electrical signals that are transmitted to the brain ([Joselevitch, 2008](#)).

Choroid: A layer of vascular tissue that exists somewhere between the sclera and the retina acts to supply the outer layers of the retina with nutrition and oxygen ([Anand-Apte and Hollyfield, 2010](#)).

2.2 Intraocular Pressure

The positive gauge pressure that is formed by the aqueous humor in the anterior chamber of the eye is known as intraocular pressure (IOP), the pressure exerted by the fluid inside the eye against its outer wall. This pressure, measured in millimeters of mercury [mmHg], plays a crucial role in maintaining the structural integrity of the eye and ensuring optimal ocular function. It is important for maintaining the shape of the eye and ensuring proper function of the optic nerve ([Zouache et al., 2016](#)). Several factors influence intraocular pressure levels, including the production and drainage mechanism of aqueous humor ([Tamm et al., 2015](#)). A proper balance between them is critical to maintaining the IOP at a standard - physiological - level.

The normal range of intraocular pressure generally falls between 10 and 21 mmHg ([Machiele et al., 2018](#)). An IOP 15 mmHg indicating that the pressure of the fluid is 15 mmHg greater than the pressure in the atmosphere. Throughout the day-night cycle,

it also fluctuates, typically peaking in the morning due to the extended period spent lying down ([Downs et al., 2011](#)). It has also been proved that the cardiac cycle affects the IOP ([Jin et al., 2018](#), [Schmidl et al., 2011](#), [Januleviciene et al., 2006](#)).

Changes in intraocular pressure can indicate conditions such as glaucoma, where the increased pressure, reaching the values as high as 35 mmHg and even higher ([Bengtsson et al., 2007](#)), can damage the optic nerve and lead to vision loss if not treated. Subsequent to cataracts, glaucoma is currently the second most widespread leading reason for blindness ([Allison et al., 2020](#)). The measurement methods involve using a device called a tonometer, which either touches the cornea or jets a puff of air onto its surface to assess IOP ([Brusini et al., 2021](#), [Da Silva and Lira, 2022](#)). Given that tonometry is an indirect technique, the measurements obtained are influenced at some level by the biomechanical properties of the eye ([Doughty and Zaman, 2000](#)). However, I hope to find a new reliable biomarker that can provide more precise and individualized assessments of IOP.

2.3 Crystalline Lens Wobbling

The so-called lens wobbling or overshooting, or oscillatory inertial movement of the crystalline lens, that originates from a rapid saccadic movement of the entire eyeball while shifting the direction of gaze, is one of the most fascinating dynamical phenomena that can be found in the eye. After the first qualitative observation of lens wobbling in the 30's of the XX century ([D'Ombraïn, 1936](#)) and then in 1970 ([Bartholomew, 1970](#)), its real quantitative description was presented by ([Jacobi and Jagger, 1981](#)) while investigating the intraocular lens (IOL) wobbling in pseudophakic eyes. Wobbling effect can be captured indirectly by means of Purkinje imaging techniques ([Tabernero and Artal, 2014](#), [Nyström et al., 2015](#)).

2.3.1 Experimental Studies

Experimental studies are fundamental in scientific research that involve the manipulation of variables to establish cause-and-effect relationships. Researchers begin with a hypothesis and design experiments to manipulate independent variables, subsequently measuring the effects on the dependent variables. However, there are limitations, such as difficulty in controlling all variables and ethical constraints, particularly with respect to experiments involving human subjects. Several studies exploring the dynamics of the crystalline lens have been documented ([Nyström et al., 2015](#), [Gambra et al., 2013](#), [Boszczyk et al., 2023](#)).

One notable aspect of these studies is the investigation of the wobbling effect, including the instrumentation used to describe it. Purkinje imaging, used by Taberero and adapted by our research group, is one of the prevailing techniques employed ([Taberero and Artal, 2014](#)).

Our research studies conducted by Visual Optics Group are categorised into two main groups: *ex vivo* (conducted outside of a living organism) and *in vivo* (conducted within a living organism). *In vivo* techniques are challenging, so most research endeavours have leaned towards *ex vivo* studies. The combination of experimental studies, alongside biomechanical models, is highly valuable for analysing vision mechanisms. ([Boszczyk et al., 2023](#), [Dahaghin et al., 2024a](#)).

2.3.2 Purkinje Imaging

Purkinje imaging refers to a technique used to visualise the reflections of light from different interfaces within the eye. Named after the Czech anatomist Jan Evangelista Purkinje, who was the first to describe these reflections in the 19th century, this optical imaging method utilises modern instrumentation, such as aberration-free lenses and high-speed cameras to capture high-resolution images.

The Purkinje images, labelled PI-PIV, are as follows (Figure 2):

PI: being the specular reflection from the anterior surface of the cornea.

PII: being the specular reflection from the posterior surface of the cornea.

PIII: being the reflection from the anterior, convex surface of the lens (PIII is invisible in Figure 2).

PIV: being the specular reflection from the posterior, concave surface of the lens.

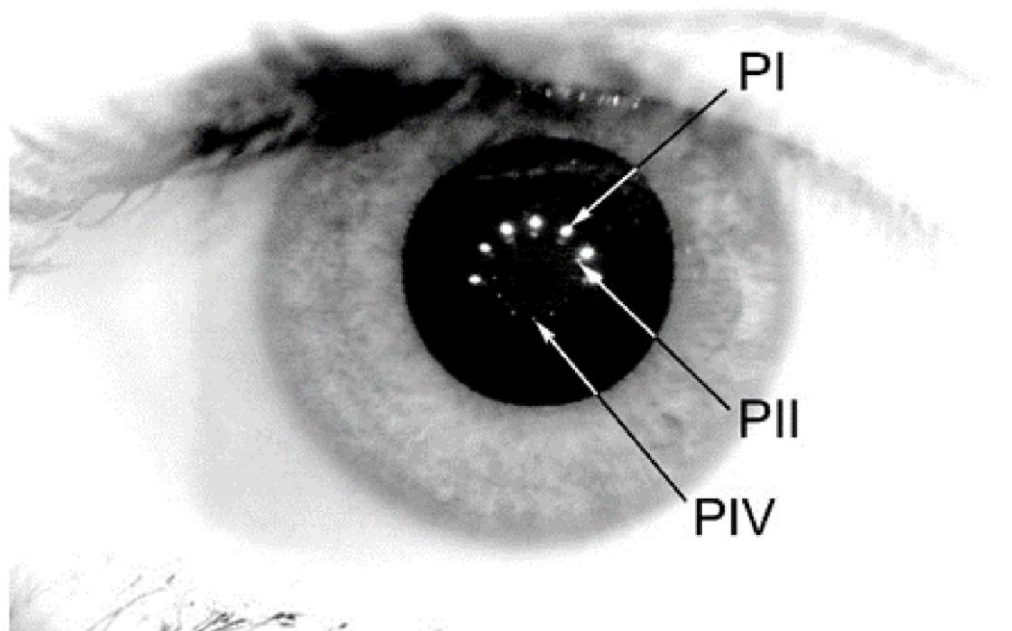


Figure 2. Purkinje images PI-PIV, PIII is indistinguishable ([Boszczyk et al., 2023](#)).

By analysing the characteristics of the Purkinje images, researchers can gain insights into various aspects of the ocular system, including the position of the crystalline lens and its arrangement within the eye due to changes in the direction of gaze ([Tabernero and Artal, 2014](#), [Tabernero et al., 2006](#)). In Figure 3, the green circles indicate the positions of the PIV lens reflections. The observed wobbling pattern refers to the relative positions between the PIV and PI reflections, not the absolute movement of PIV itself. It is essential to distinguish between these absolute and relative positions to avoid confusion. Tabernero and Artal made this clear in their work, where Figure 3 illustrates the absolute positions of both PIV and PI reflections using the Purkinje system. This, however, is different from the relative positions where the difference between PIV and PI is fitted to a harmonic oscillator model. It needs to be emphasized that they were the first to propose a quantified description of this wobbling pattern ([Tabernero and Artal, 2014](#)). The black lines in Figure 4 represent the fit of the damped harmonic oscillator model to the experimental data.

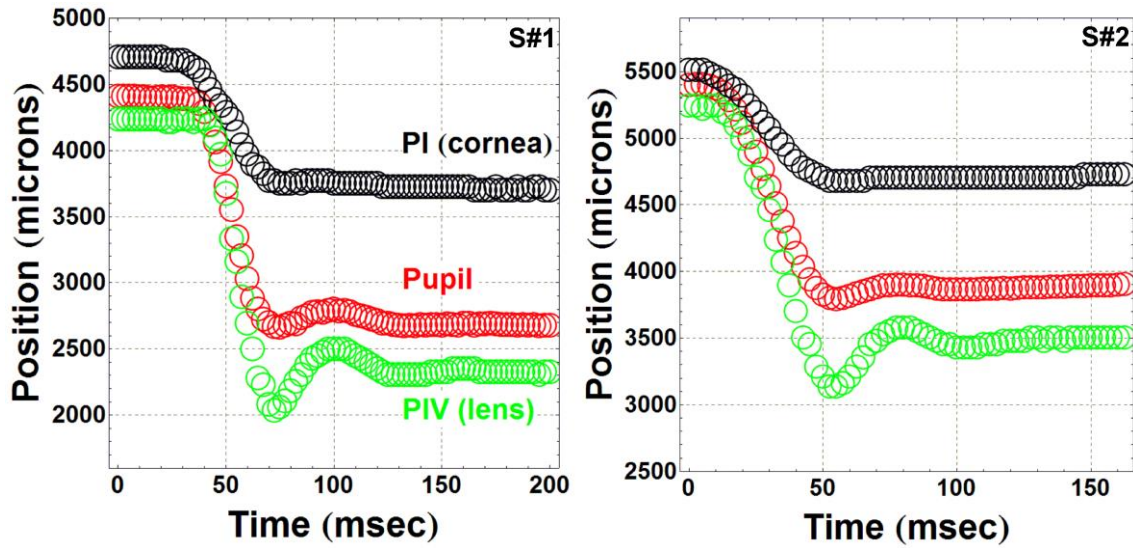


Figure 3. Tracking PI (corneal reflection) and PIV (lens reflection) positions for two different subjects. The black circles represent the stable PI positions, while the green circles track the PIV positions, which exhibit post-saccadic oscillations (Tabernero and Artal, 2014).

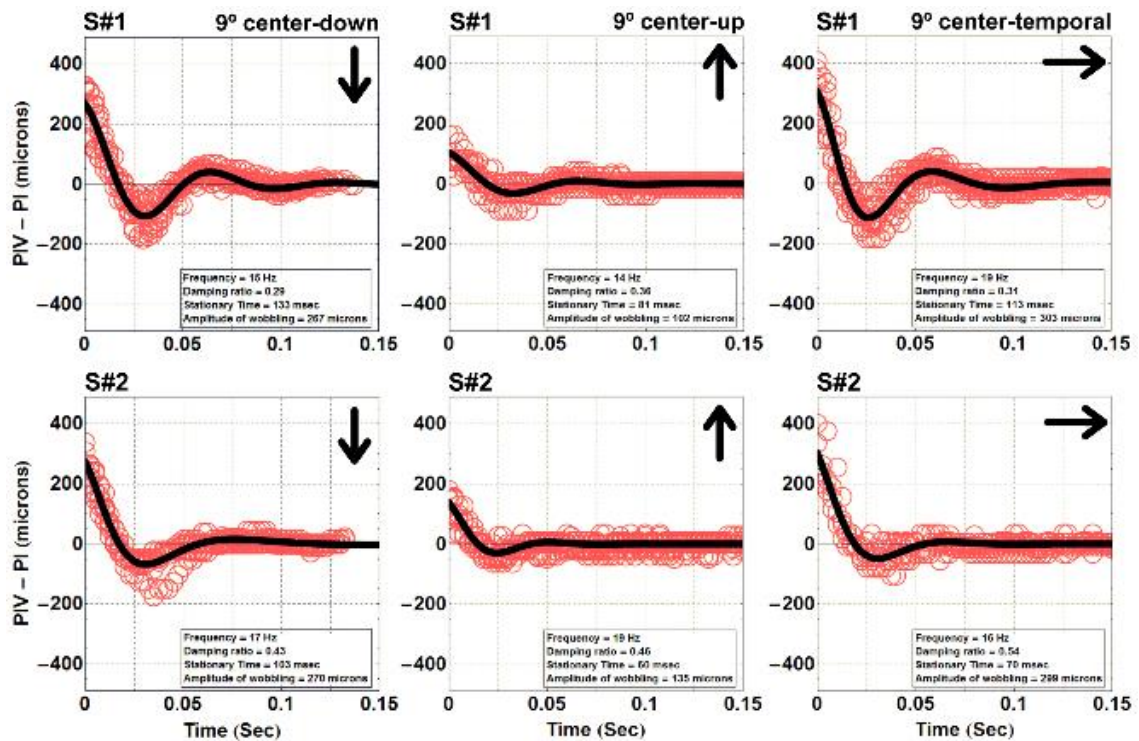


Figure 4. Wobbling data for two different subjects depending on their orientation (Tabernero and Artal, 2014).

2.3.3 Simple Harmonic Oscillator

Tabernerero and Artal identified similarities between the wobbling pattern of the lens and the behavior of a classical harmonic oscillator, using a similar mathematical framework to describe the system. A simple harmonic oscillator typically exhibits oscillatory motion, where the restoring force is proportional to the displacement from the equilibrium position and acts in the opposite direction, as expressed by Hooke's Law:

$$F = -kx \tag{1}$$

In case of crystalline lens, while the traditional components of mass and stiffness do not directly apply, the analogy comes from the behavior of the lens wobbling, which can be described by similar oscillatory principles. Instead of mass and stiffness, Tabernerero's description focuses on the displacement of the fourth Purkinje Image (PIV) relative to the first Purkinje Image (PI), and the observed wobbling is mathematically treated using the classical harmonic oscillator notation.

In real-world oscillators, damping (a force that dissipates energy) also plays a role, which is expressed through the damping ratio ζ . The damping ratio in the traditional harmonic oscillator model is given by:

$$\zeta = \frac{c}{2\sqrt{mk}} \tag{2}$$

where c represents the damping coefficient, m denotes the mass, and k indicates the stiffness of the system. However, in the lens wobbling system described by Tabernerero, no actual mass is involved. Instead, the parameters such as amplitude (the largest – in terms of magnitude – overshooting of the lens from its equilibrium position), damping ratio, and oscillation frequency are used to describe the lens's wobbling behavior without the explicit need for mass or stiffness. He captured the dynamics of the lens wobbling system by fitting those parameters for the first time ([Tabernerero and Artal, 2014](#)).

2.4 Basic Concepts in Eye Biomechanics

Like any living organism, the eye requires a series of intricate and interconnected processes to function properly. If any of these processes is disrupted, it can affect the entire visual

system. Despite advances in experimental and clinical techniques, there are still many aspects of vision that remain unrevealed. Ocular biomechanics has emerged as a solution to this challenge, focusing on the biomechanical aspects of eye function. By applying principles from physics, mathematics, and engineering, biomechanics analyzes movements, forces, and interactions within the eye during various activities. This systematic approach provides valuable information on how the eye works ([Ljubimova, 2009](#)).

Estimating how crystalline lens behaves in different conditions is not always straightforward through *ex vivo* and *in vivo* experiments alone. Modeling the eye can be convenient to supplement experimental techniques and to figure out behaviors that are intricate to replicate experimentally. In this thesis, chapters 4 and 5 present a comprehensive model of the crystalline lens, simulating its response under different material properties and physiological conditions, i.e. pressure.

The following are key terms and concepts from biomechanics that may be unfamiliar to ophthalmologists and opticians.

2.4.1 Finite Element Method

The Finite Element Method (FEM) is one of the most powerful numerical techniques to solve complex engineering problems. It is used to find approximate solutions to boundary value problems for partial differential equations. Figure 5 illustrates a schematic of its steps. FEM is rooted in the principles of variational calculus and approximation theory. By discretizing the domain into finite elements, it can simulate modern engineering systems. Then, the governing differential equations are solved on each element ([Huebner et al., 2001](#), [Maklad, 2019](#)).

Its versatility has made it indispensable in industries such as automotive, aerospace, civil engineering, and biomedical engineering. This method is adept at tackling mechanics problems involving intricate geometries, making it an ideal choice for exploring the mechanics of the eye. This technique is widely implemented in software packages such as COMSOL Multiphysics, ANSYS, and Abaqus.

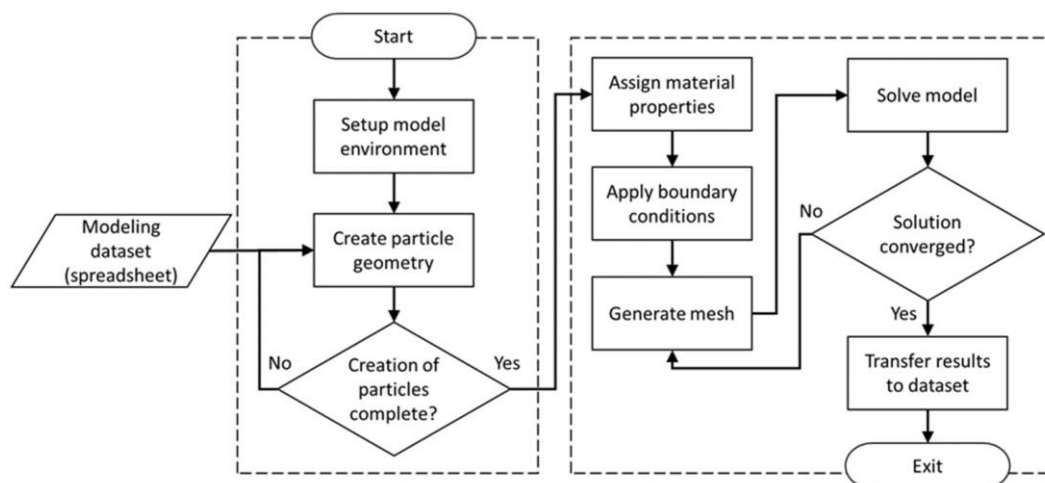


Figure 5. Schematic of the FEM steps for modeling and analysis (Moghaddam and Mertiny, 2019).

FEM models offer a significant benefit in biological research by potentially decreasing the need for experimental tests, thereby preventing ethically ambiguous situations. Nevertheless, oversimplifications along with overlooking the effective parameters are the main problem in the FEM approach (Markov, 2020).

2.4.2 Mesh Generation

In discretization, the domain is divided into finite elements and the boundary conditions are applied to each element individually. Mesh generation is a critical step in FEM, where a well-structured mesh ensures accurate results and efficient computation. Using a large number of elements leads to more precise solutions, albeit at the expense of increased computational time.

Different types of elements are used to accurately represent the geometry and behavior of the system. Common element types include triangular or quadrilateral meshes for 2D problems and tetrahedral or hexahedral meshes for 3D problems (Figure 6). These elements are linked at particular points known as nodes, and the solution for the field variable is determined solely at these nodes (Genest, 2010).

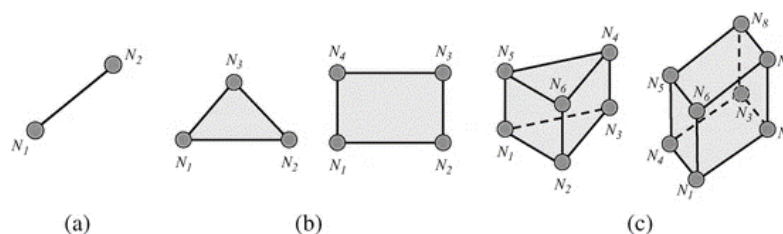


Figure 6. Element dimensions for (a) 1D, (b) 2D and (c) 3D elements (Okereke et al., 2018).

2.4.3 Mechanical Properties

Tension tests are commonly employable to determine the elastic properties of many different materials ([Genest, 2010](#)). Figure 7 shows the stress-strain curve obtained by tension tests typically used in materials science and engineering, this curve helps to characterize the mechanical properties of a material. The tension test is a method used to determine the mechanical properties of materials by subjecting specimens to stretching on a hydraulic testing systems. As the specimen stretches, the force applied and the resulting elongation are measured and converted into stress and strain values. While this section presents general mechanical properties to illustrate basic concepts in mechanics, the specific values relevant to the structures of the eye are provided in Table 2 (Chapter 3) for the porcine eye, and in Table 11 (Chapter 6) for human eye.

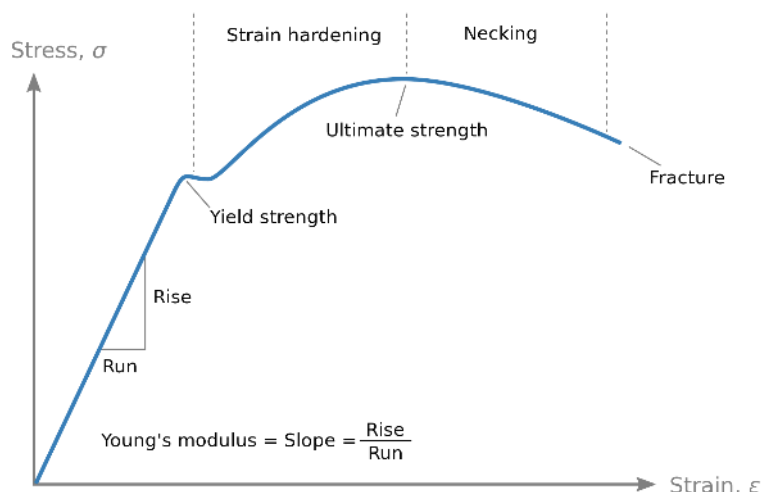


Figure 7. Typical stress–strain curve ([Nicoguardo, 2020](#)).

2.4.3.1 Linear elasticity

The initial part of the stress-strain curve is known as the elastic region. In this phase, the materials exhibit elastic behavior, which is governed by Hooke's law. According to this law, stress is directly proportional to the strain within the elastic limit, meaning that materials regain their original shape once the applied load is removed ([Courtney, 2005](#)).

Young's modulus

Young's modulus, also known as the modulus of elasticity or the elastic modulus, is a measure of the stiffness of a material. It quantifies the ability of a material to deform under stress along an axis when subjected to axial (tensile or compressive) forces ([Genest, 2010](#)).

The pressure units commonly employed to express Young's modulus are pounds per square inch [psi] and Pascals [Pa]. It reflects how much a material will elongate or compress under a given load. Mathematically, it is expressed as the ratio of the change in length to the original length divided by the applied force. It is represented by the equation (3):

$$E = \frac{\Delta\sigma}{\Delta\varepsilon} \quad (3)$$

where E is Young's modulus, $\Delta\sigma$ stands for stress change and $\Delta\varepsilon$ represents strain change. The stress is defined as follows:

$$\sigma = \frac{F}{A_0} \quad (4)$$

where F is the force, and A_0 is the initial cross-sectional area and strain change. The following equation can be used to obtain strain:

$$\varepsilon = \frac{\Delta L}{L_0} \quad (5)$$

where ΔL is the elongation, and L_0 is the initial length. Several factors influence Young's modulus, including temperature and pressure. Materials with high Young's modulus values are stiff and resist deformation, whereas those with low values are more flexible and deform easily under load. Young's modulus is an essential property used in biomechanical design and analysis ([Knudson and Knudson, 2007](#), [Özkaya et al., 2017](#)).

Poisson's ratio

The ratio of axial strain to transverse strain is known as Poisson's ratio. Imagine stretching a rubber band: as you pull it lengthwise, it gets thinner sideways. Poisson's ratio quantifies this relationship and is mathematically defined as the negative ratio of the transverse strain. It is denoted by the symbol ν (nu):

$$\nu = -\frac{\varepsilon_{transverse}}{\varepsilon_{axial}} \quad (6)$$

Poisson's ratio is a dimensionless quantity and complements other mechanical properties, such as Young's modulus, typically ranging between -1 and 0.5 for most engineering materials. A negative Poisson's ratio implies lateral expansion under tension, while a positive Poisson's ratio indicates that a material contracts laterally when stretched. Several factors influence it, including composition, temperature, pressure, and microstructural characteristics ([Knudson and Knudson, 2007](#), [Özkaya et al., 2017](#)).

2.4.4 Boundary Conditions and Governing Equations

At the core of the finite element method lies the notion of boundary conditions which determine how the system interacts with its surroundings. These conditions act as a link between the simulated environment and the real-world situation, establishing the limits and forces exerted on the system, thus shaping its behaviour and the precision of the analysis. Boundary conditions restrict the system behaviour during analysis, mirroring the physical limitations or external impacts affecting it. They specify the values of variables (like pressure, velocity, temperature) at the edges of the computational domain. Boundary conditions are pivotal in ensuring that simulations faithfully represent real-world situations. Attaining precise and dependable simulation outcomes necessitates thoughtful consideration and application of boundary conditions ([Whiteley, 2014](#)).

When considering the *in silico* reconstruction of *ex vivo* and *in vivo* experiments, it is important to recognize that these experiments were conducted under different conditions, leading to distinct boundary conditions in the simulations. The relationship between boundary conditions and experimental constraints is essential, as accurate simulations must replicate the conditions of the physical experiments to ensure validity.

The fluid dynamics around the eye are described by the time-dependent Navier-Stokes equations ([Dahaghin et al., 2024a](#)):

$$\rho \frac{\partial \mathbf{v}}{\partial t} + \rho \nabla \cdot (\mathbf{v} \otimes \mathbf{v}) - \mu \nabla^2 \mathbf{v} + \nabla p = \rho \mathbf{f}, \nabla \cdot \mathbf{v} = 0 \quad (7)$$

where \mathbf{v} is the fluid velocity, p is the pressure, \mathbf{f} represents volumetric forces, ρ is the density, and μ is the dynamic viscosity.

The mechanical behavior of the eye during rotation is modeled using multibody dynamics, as described by the following equation:

$$\rho \frac{\partial^2 \mathbf{u}}{\partial t^2} = \nabla \cdot (\mathbf{FS})^T + \rho \mathbf{f}, \mathbf{F} = \mathbf{I} + \nabla \mathbf{u} \quad (8)$$

where u is the displacement field, F is the deformation gradient tensor, S is the second Piola-Kirchhoff stress tensor, and I is the identity matrix.

The interactions between the fluid and solid components are captured using a fully coupled FSI approach, ensuring synchronized updates of the fluid and solid parameters.

$$\mathbf{f}_a = [-p\mathbf{I} + (\mu (\nabla \mathbf{v} + (\nabla \mathbf{v})^T) - 2/3 \mu (\nabla \cdot \mathbf{v})\mathbf{I})] \cdot \mathbf{n}, \mathbf{v} = \frac{\partial \mathbf{u}_{\text{soli}}}{\partial t} \quad (9)$$

Detailed descriptions of the corresponding boundary conditions can be found in the materials and methods sections of Chapters 3 and 6.

2.5 Optics of the Eye

Physiological optics is an emerging branch of physics that deals with the study of light as it relates to the human eye. Human eye is a masterpiece of biological engineering; from the transparent cornea to the light-sensitive retina, every component contributes to the formation of clear and focused images. Similar to a camera, with its cornea as the primary refracting element, pupil as a changeable aperture, crystalline lens for adjustable focusing, and posterior chamber as a dark area ([Chen and Stojanovic, 2017](#)). Key concepts in eye optics include refraction, accommodation, and the function of the lens and cornea in focusing light onto the retina. Refraction, the bending of light as it passes through different mediums, is essential for proper vision. By refracting light rays, the eye can adjust its focus to accommodate objects at varying distances.

In addition, the eye adjusts its ability to focus on nearby objects through another process known as accommodation. This occurs when the crystalline lens alters its optical power ([Chien et al., 2006](#)). When light enters the eye, it passes through the cornea, pupil, and lens, undergoing refraction at each stage to focus the incoming rays onto the retina.

In my research, the optics of the eye was further explored through the integration of biomechanical and optical simulations. Reliable estimation of the optical parameters, including geometry, is crucial for investigating the optical performance and quality of vision. While the optical parameters of the cornea and aqueous humor are relatively easy to measure

due to their location in the anterior part of the eye, investigation of the crystalline lens presents more challenging and provides more dispersed/scattered data.

Table 1. Eye model parameters in which age and accommodation stimulus are included as variables (Zapata-Díaz et al., 2019).

Surface	Radius (mm)	Central thickness to next surface (mm)	Refractive index	Asphericity
Anterior corneal surface	7.87	0.574	1.376	$-0.24 + 0.003 \times \text{Age}$
Posterior corneal surface	6.40	-	-	$-0.006 \times \text{Age}$
Aqueous	-	$3.296 - 0.010 \times \text{Age} + A \times (-0.048 + 0.0004 \times \text{Age})$	1.336	-
Anterior lens surface	$1/[1/(12.9 - 0.057 \times \text{Age}) + 0.0067 \times A]$	$2.93 + 0.0236 \times \text{Age} + A \times (0.058 - 0.0005 \times \text{Age})$	$1.441 - 0.00039 \times \text{Age}$	$-6.4 + 0.03 \times \text{Age} - 0.5 \times A$
Posterior lens surface	$1/[1/(-6.2 + 0.012 \times \text{Age}) - 0.0037 \times A]$	-	-	$-6 + 0.07 \times \text{Age}$
Vitreous	-	-	1.336	-

The lens is a gradient structure, with its refractive index varying as a function of spatial coordinates. Additionally, its shape and gradient index profile are subject to changes with accommodation and age, complicating the analysis further. This complexity has led to the

development of various models of the human eye, including those representing both relaxed and accommodated states ([Atchison and Thibos, 2016](#), [Navarro et al., 1985](#)), as well as several models focused solely on the lens ([Pierscionek, 1993](#), [Smith et al., 1991](#), [Urs et al., 2010](#)), based primarily on *in vitro* measurements.

For the purpose of the research presented in this thesis, I utilized a generic model deemed most convenient: the Zapata-Diaz model. In particular, I employed this geometric data for FEM simulations, customized for a particular age and state of accommodation (Table 1). A detailed discussion of this approach will be provided in Chapter 6. ([Zapata-Díaz et al., 2019](#)).

The biomechanical simulations relied solely on the implementation of this model's geometry. While my primary responsibility lay in the mechanical simulations, the numerical workflow I co-authored, combined these two fields to better understand the mechanical and optical behavior of the eye in terms of mechanical inertial re-arrangement of the lens within the eye and optical performance in terms of Purkinje imaging being the optical manifest of this mechanical re-arrangement.

2.6 Experimental Inspiration for Biomechanical Simulations

The experimental investigations by means of optical instrumentation and methods conducted by members of the Visual Optics Group at Wrocław University of Science and Technology serve as both the motivation for the biomechanical simulations and as the means to validate the developed models. Using their results was essential for establishing a framework upon which the simulations were built. This also ensures the accuracy of the developed model and emphasizes confidence in its reliability.

2.6.1 *Ex vivo* Experiment

In the *ex vivo* experiments, the Purkinje performance was evaluated in relation to eye rotation using a porcine eye shortly after slaughter. A custom setup was employed featuring a holder for the eye mounted on a high-speed precision rotation stage, which allowed for controlled angular movements. An infrared illuminator was strategically positioned in front of the eye, which underwent rotations of up to 90 degrees at high speeds of 1,700 degrees per second and accelerations reaching 60,000 degrees per squared second, which is the order of magnitude of the peak angular acceleration of a living human eye while its natural motion ([Zhang et al., 2012](#)). The Purkinje images were captured using a high-resolution FastCam

Mini UX50 camera, and five sequences of these images were subsequently analyzed (Figure 8) ([Dahaghin et al., 2024a](#)).

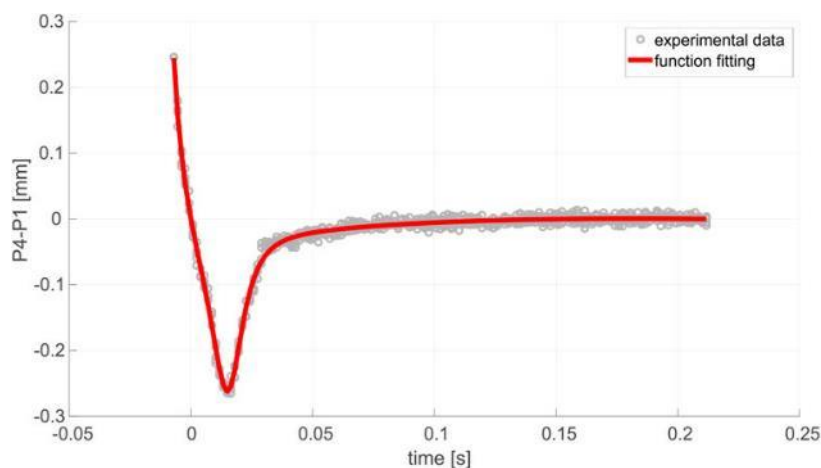


Figure 8. Overshooting effect observed in the examined eye ex vivo ([Dahaghin et al., 2024a](#)).

2.6.2 *In Vivo* Experiment

For the *in vivo* data collection, the experimental setup was incorporated, similar to the Dynamic Purkinje-meter developed by ([Taberero and Artal, 2014](#)). This setup was enhanced by integrating a 1.3-megapixel CMOS image sensor within a FASTCAM Mini UX50 camera, which enabled high-quality Purkinje image capture at 640 frames per second. Additionally, a semicircular illuminator equipped with seven infrared diodes (operating at a wavelength of 850 nm) was positioned approximately 12 cm in front of the eye. The subjects were instructed to follow a fixation target both before and after undergoing a water drinking test (WDT). WDT is a clinical assessment used to evaluate intraocular pressure (IOP) in individuals at risk for glaucoma. During the test, a patient drinks a specified amount of water within a short time, after which IOP measurements are taken at regular intervals ([Przeździecka-Dołyk et al., 2021](#)).

Empirical data collected during these experiments (Figure 9 and Figure 10) have not been publicly revealed yet and some of them have been submitted and are still waiting for reviews and publication. For a comprehensive overview of the submitted manuscripts, please refer to the “Submitted Manuscripts” section within the Activities During the PhD Period 2021-2024 (Pages vi-vii).

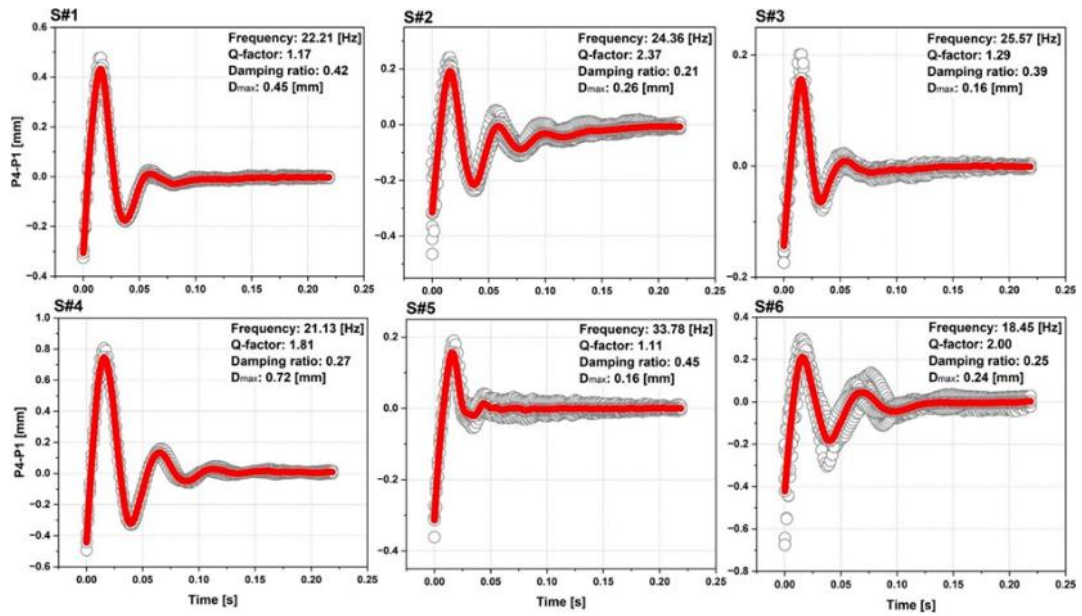


Figure 9. Wobbling patterns for six different subject (physiological IOP)(sourced from the submitted manuscripts).

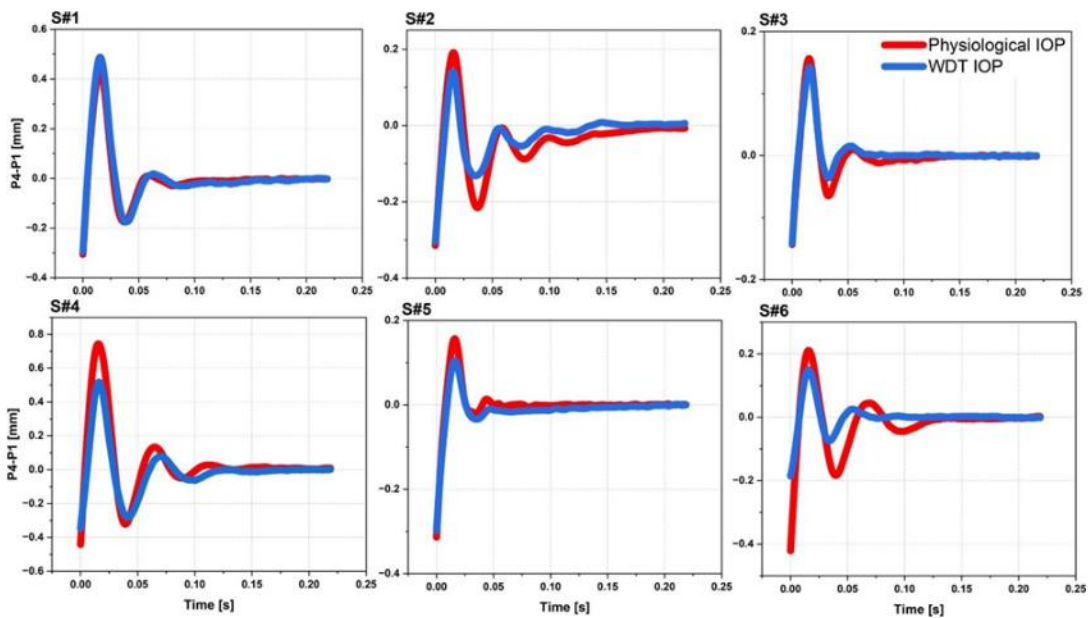


Figure 10. Comparison of wobbling patterns for six different subjects, illustrating both physiological IOP and post-WDT measurements (sourced from the submitted manuscripts).

Chapter 3

In silico Reconstruction of *Ex vivo* Experiment

3.1 Research highlights

- 1 The crystalline lens shifts excessively after eye rotation stops.
- 2 Highlights the need to understand the dynamics of the eye for accurate predictions.
- 3 Establishes parameters for *ex vivo* simulations, minimizing the need for extensive experiments.

3.2 Introduction

The lens undergoes inertial motion due to its fast rotation followed by a sudden stop. This wobbling effect was first noticed qualitatively by ([D'Ombraïn, 1936](#)). A recent study ([Boszczyk et al., 2023](#)) suggested that this wobbling involves two main movements: lateral displacement and tilt, both of which have a significant impact on recorded and simulated Purkinje images of the eye. A comparable effect was also reproduced in a mechanical model of intraocular lens implants ([Martin et al., 2009](#)). Despite this, there has been no in-depth investigation of this phenomenon through *ex vivo* experimental or numerical studies.

Studying the porcine eye *ex vivo* is important because it addresses challenges in obtaining accurate data or modifying parameters in *in vivo* tests. This chapter aims to advance understanding of the crystalline lens's dynamic behavior during rapid eye movement, contributing to insights on the wobbling phenomenon and developing an *ex vivo* optomechanical model for future research.

3.3 Materials and Methods

A two-dimensional numerical model using COMSOL Multiphysics was developed to study the inertial motion of the crystalline lens in a porcine eye globe ([Dahaghin et al., 2024a](#)). While three-dimensional models are typically employed in such studies, a 2D approach was chosen here due to its computational efficiency and sufficient accuracy for planar rotational motion, where the dynamics can be effectively captured without the added complexity of a 3D model. The motions occurs primarily within a single plane, allowing for the neglect of the out-of-plane dimensions. This simplification is particularly advantageous as the model requires outcomes to be sampled densely in time to accurately capture dynamic effects. Additionally, the axis of rotation is perpendicular to the plane of the model, reinforcing the appropriateness of a 2D representation.

The model incorporates key eye components like the crystalline lens, vitreous body, aqueous humour, zonular fibers, cornea, sclera, and ciliary muscle (Figure 11 A). Geometrical dimensions are based on existing literature ([Regal et al., 2021](#), [Menduni et al., 2018](#)), excluding the thin choroid and retinal layers due to their minimal impact.

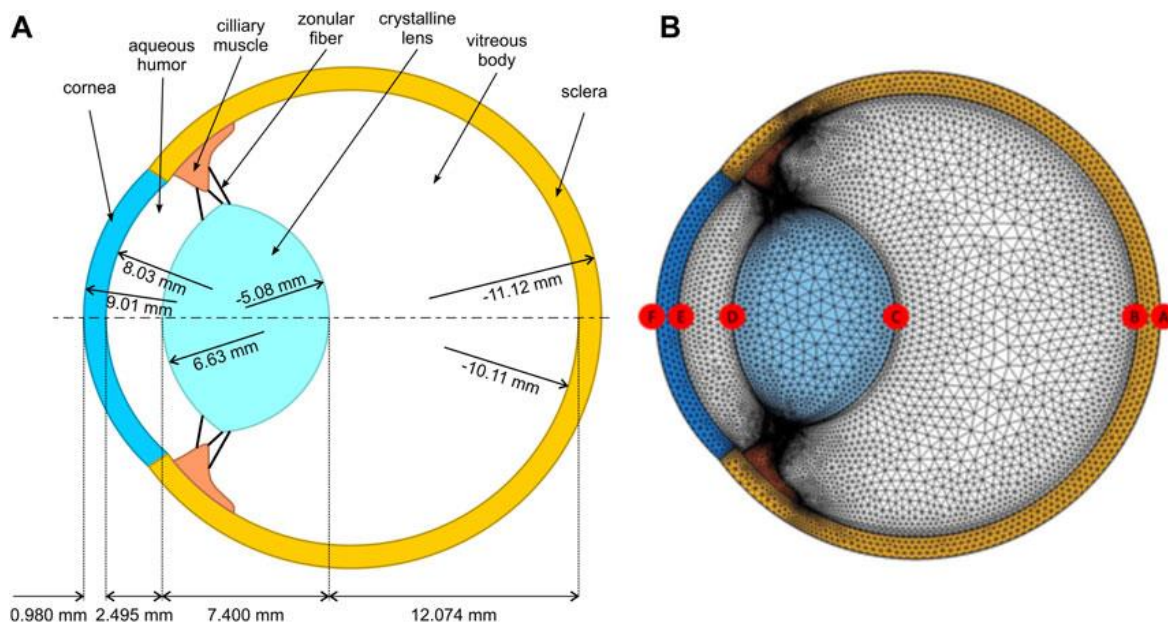


Figure 11. (A) Dimensions of the finite element model. (B) Mesh arrangement (Dahaghin et al., 2024a).

The eyeball model was rotated 90 degrees around its vertical axis, which is perpendicular to the plane of the two-dimensional model, while data were collected for the movement of the apical points of the crystalline lens (see points C and D in Figure 11 B) to estimate the dynamics of the lens arrangement within the eye globe. This analysis allows for the extraction of the tilt and lateral dislocation components.

During the smooth rotation, the eye reached a peak angular velocity of 1,700 degrees per second (see paragraph 2.6. *Experimental inspiration for biomechanical simulations* for details). Additionally, the pivot point for the rotation, positioned at the center of the eye globe, was fixed 11.82 mm from the anterior cornea, with no linear displacement.

To accommodate the irregular geometry, triangular elements (as shown in Figure 11 B) were employed to discretize both the solid and fluid domains. The model comprised a total of 48,139 elements, with an average element quality rating of 0.82. This quality rating, which ranges from 0 to 1, was determined using the built-in quality assessment tool based on equiangular skew (Etminan et al., 2023). The chosen mesh size was deemed optimal following a sensitivity analysis and observed that reducing the mesh size in the program did not significantly affect the outcomes.

All elements of the model were assumed to exhibit linear elastic behavior, with distinct material properties based on data reported in previous research. Table 2 provides the corresponding values for each of the components. Vitreous body and aqueous humour are modeled as a viscous Newtonian incompressible fluid. For this media, dynamic viscosity and density are of 0.00074 Pa·s and 1000 kg/m³ respectively (Singh et al., 2017).

Table 2. Material properties of the porcine eye ([Watson et al., 2015](#), [Wang et al., 2017](#)).

modelled parts	Young's modulus [MPa]	Poisson's ratio [-]	Density [kg/m ³]
Sclera	28	0.49	1400
Cornea	12	0.48	1400
Ciliary Muscle	11	0.45	1600
Lens	1.5	0.49	1100
Zonule fibres	0.95	0.49	1000

To evaluate whether the mechanical model is able to mimic the behavior of a real eye, it was essential to establish the correlation between the positions of the Purkinje images and the actual alignment of the crystalline lens. For this analysis, the method outlined by ([Boszczyk et al., 2023](#)) was used.

The same geometry was used as an input into the Zemax Optic Studio, a widely-used optical design software that enables to simulate the optical performance through various optical systems. This software allows for precise modeling of optical components, including tilted and decentered lenses and mirrors. For this simulation, the refractive indices for an 850 nm wavelength were used, cornea (1.3643), aqueous humor (1.3252), and lens (1.4617), as reported by ([Wong et al., 2007](#), [Sanchez et al., 2011](#)). The relationship between the relative Purkinje distance and tilt and decentration can be approximated to a three-dimensional plane:

$$\Delta x_{PIV-PI} = -0.000112 + 0.01977 \cdot tilt - 1.097 \cdot dec \quad (10)$$

where Δx_{PIV-PI} is expressed in millimeters, *tilt* is expressed in degrees, and decentration (*dec*) is expressed in millimeters. This equation was employed to assess Purkinje performance by utilizing lens alignment data, which had been generated through dynamic simulations. This approach follows the procedure outlined in a prior study by ([Boszczyk et al., 2023](#)).

3.4 Results

To ensure the validity of the models used in this study, I used experimental data obtained from previous research conducted by the Visual Optics Group at Wrocław University of Science and Technology. In particular, Figure 8 in chapter 2 illustrates the curve fitting of the experimental data, highlighting the accuracy and precision of the model employed.

Figure 12 shows a set of characteristic parameters in the evolution of PIV-PI. Y_{Peak} represents the maximum overshooting amplitude, while $t_{1/2}$ and $t_{1/4}$ denote the widths at half and quarter depths of the overshooting pattern, respectively.

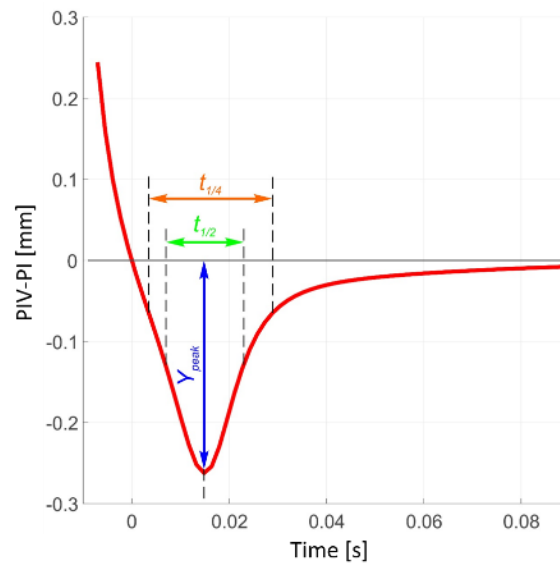


Figure 12. Parametrization of the overshooting trajectory ([Dahaghin et al., 2024a](#)).

In Figure 13, we illustrate the variations in the apex position of the lens relative to the center of the cornea over time, comparing both experimental and modeling results. The data reveal that the maximum overshoot observed in the experimental results is notably similar to the corresponding value found in the modeling results. This correlation suggests that the model enables to effectively reproduce the dynamics of the lens behavior.

To further analyze this, I present in Table 2 the parameters that define the dynamic response of the lens, as predicted by the model alongside the findings from the experimental tests. The errors are relatively modest, measuring at 13.92% for $t_{1/2}$ s, 5.50% for Y_{Peak} mm, and 1.59% for $t_{1/4}$ s. These error percentages indicate that the model's predictions are quite accurate, reinforcing the reliability of the results obtained from theoretical approaches.

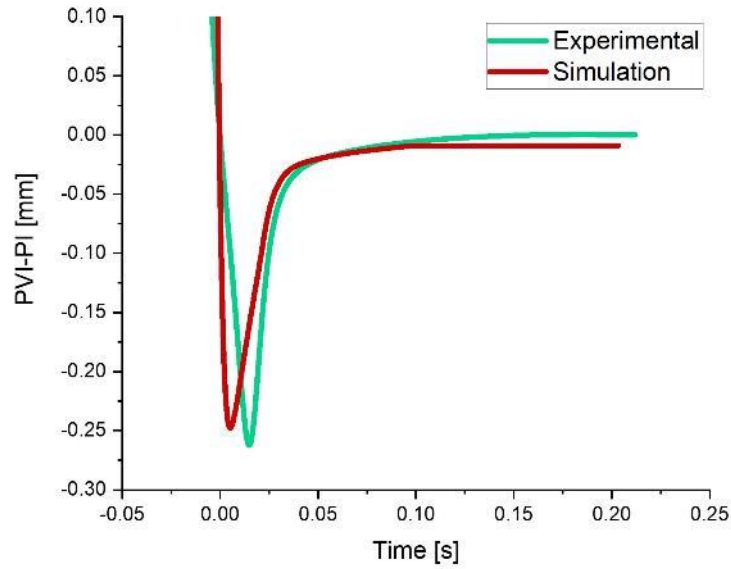


Figure 13. Overshooting magnitude in the experimental and simulation results ([Dahaghin et al., 2024a](#)).

Table 3. Detailed data related to the errors.

	Y_{peak} [mm]	Relative error	$t_{1/2}$ [s]	Error	$t_{1/4}$ [s]	Relative error
Experimental	-0.2621		0.0158		0.0252	
		5.50%		13.92%		1.59%
Simulation	-0.2477		0.018		0.0248	

Figure 14 presents the optimization of the damping factor function, which employs a diverse range of trends and values for the damping factor. The goal of this optimization is to ensure that the displacement pattern closely resembles the experimental graph.

Analyzing the figure reveals that the damping effect increases steadily up to 0.125 seconds. Following this point, the damping reaches its highest level as the lens faces the greatest resistance at its peak position. This behavior is crucial for accurately modeling the system's response and aligns with the observed experimental data, highlighting the importance of fine-tuning the damping factor to achieve a more precise representation of the dynamics involved.

Table 4 presents the data achieved from the eye's damping functions within the numerical model: $t_{balance}$ (stabilization time), C_{max} (maximum damping), C_{end} (damping at the end), C_{min} (minimum damping), ΔC , and ΔC_{max} .

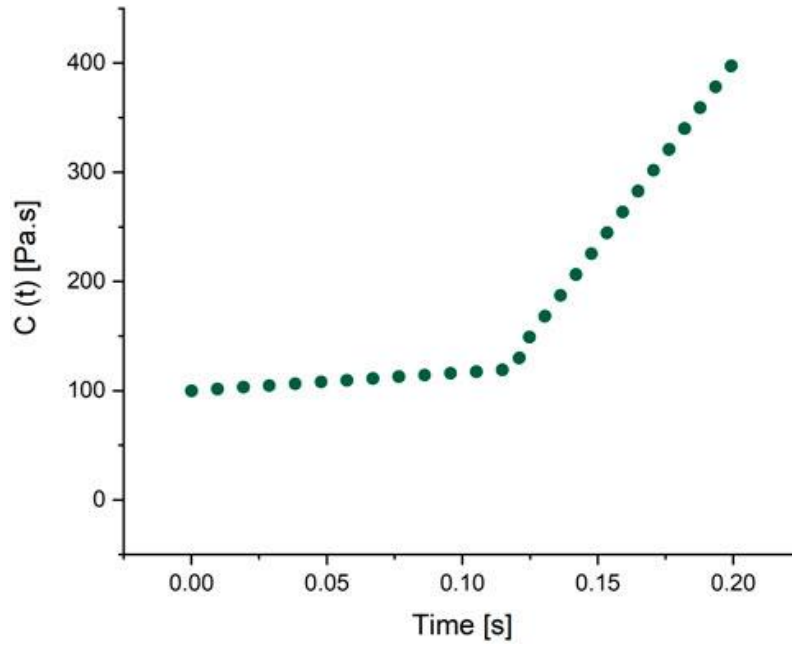


Figure 14. Damping function ([Dahaghin et al., 2024a](#)).

Table 4. Damping data.

$t_{balance}$	C_{max}	C_{end}	C_{min}	C_{start}	ΔC	ΔC_{max}
[s]	[Pa·s]	[Pa·s]	[Pa·s]	[Pa·s]	[Pa·s]	[Pa·s]
0.2	400	400	5	100	300	395

3.5 Discussion and Conclusions

In an *ex vivo* setup, where the eye is studied outside of a living organism, it is assumed that the eye is in a state of full relaxation, meaning it is not focusing on any particular object. The zonules are under tension in this state. This tension plays a crucial role in minimizing the movement of the lens when the eye is rotated. As a result, our findings differ from earlier studies conducted within living organisms ([Tabernero and Artal, 2014](#)), where the lens exhibited periodic oscillations or wobbling. In our *ex vivo* experiments, such oscillations are absent. Instead, the lens movement follows a distinct pattern, as illustrated in Figure 13.

This observed behavior can be attributed to the lens initially moving beyond its intended position after a sudden halt. Over time, the lens gradually stabilizes, a process

influenced by the damping effect provided by the zonules. This damping effect helps to absorb the excess motion and bring the lens to a steady state.

It is crucial to acknowledge that our two-dimensional model has some limitations. One significant limitation is the exclusion of the turnover outflow at the trabecular meshwork, which is a part of the eye's drainage system. Addressing this aspect in future research could provide a more comprehensive understanding of the lens dynamics.

Chapter 4

In silico Evaluation of the Material Effects

4.1 Research Highlights

- 1 Material properties influence the crystalline lens overshooting during eye rotation.
- 2 Fine-tuning zonules material properties for reliable modelling is important.
- 3 Despite varied material properties, the timing of maximum overshooting remains relatively constant.

4.2 Introduction

Research on crystalline lens overshooting is progressing rapidly, especially in terms of understanding its maximum displacement and stabilization time. In previous section, a pioneering study was discussed that, to the best of our knowledge, for the first time crystalline lens overshooting was modeled as a quantifiable effect of inertia under *ex vivo* conditions ([Dahaghin et al., 2024a](#)). It provides fresh insights into lens behavior, deepening our understanding of its dynamics within the eye. By employing computational methods, scientists can simulate, analyze, and predict the complex structural behavior of the eye ([Zhou et al., 2017](#)). This technique provides valuable insights into the mechanical properties of the eye and its reactions to external forces, serving as a dependable alternative to *in vivo* studies while maintaining high accuracy. Consequently, this research marks a significant advancement in ocular science.

Emerging challenges can cast doubt on established findings and assumptions. For instance, recognizing that a wide range of factors significantly influence the eye biomechanics implies that efforts should focus on narrowing these factors. A major difficulty is the inconsistency of captured or estimated data, often resulting from intersubject variability. Every individual's eye possesses distinct features, such as differences in material properties and dimensions, along with varying physiological and environmental factors, which can greatly affect the outcomes. Furthermore, the variety in eye characteristics requires a more individualized approach to studying and simulating eye biomechanics. Researchers need to consider how specific material properties, such as corneal elasticity or intraocular pressure, differ between individuals. Additionally, some environmental factors, such as lighting conditions and exposure to pollutants, can impact eye behavior and health. Addressing these variables is essential for creating accurate and reliable computational models for both research and clinical purposes. Therefore, future studies should aim to develop methods that account for this variability, potentially leading to more personalized and effective treatments for eye conditions ([Coldrick, 2013](#), [Ayyalasomayajula et al., 2016](#), [Issarti et al., 2021](#)).

The material properties of the ocular tissues play an important role in numerical analysis, significantly influencing the accuracy and outcomes of the models. It is crucial to examine these properties using the most precise available data. This analysis ensures that research results are not only realistic but also dependable. To achieve these goals, it is

imperative to obtain accurate material properties of ocular tissues. The accuracy of FEM simulations relies heavily on material input to validate the model predictions. Therefore, the acquisition and integration of precise material properties represents a crucial advancement in ocular biomechanics, enabling more insightful studies in the years ahead.

The main goal of this chapter is to assess the crystalline lens overshooting response due to variations in the material properties of ocular structures. This expanded analysis involves a detailed examination of the unique contribution of each structure to the behavior of the crystalline lens. Considering the varied mechanical properties documented in the literature for eye components, this part recognizes the substantial influence each can exert on the results by adjusting the material properties within their reported ranges. In other words, this method underscores the lens sensitivity to individual structural changes. In summary, the research produces a reliable *in silico* model, which serves as a tool for simulating and predicting the optomechanical responses of the eye in a controlled *ex vivo* setting in future research.

4.3 Sensitivity Analysis

In FEM, the sensitivity analysis examines how variations in input parameters influence the outputs. By altering factors such as geometry, material properties, boundary conditions, mesh size, and applied loads, one can evaluate their impact on the model outcomes. This information is crucial for model validation, as it highlights where precision in parameter estimation is most needed and aids in understanding which inputs the model is most sensitive to, thereby identifying key parameters that significantly affect its behavior. Parameters that cause substantial changes in the output are deemed sensitive, while those that have little effect can be considered less critical ([Lund, 1994](#)). Figure 15 shows the sequential steps required to perform a sensitivity analysis, illustrating the workflow from parameter selection through to the interpretation of results.

In order to assess the influence of material properties on the crystalline lens overshooting amplitude, an optomechanical model, which was previously developed and calibrated using Purkinje images performance in Chapter 3, was used, and all settings were adjusted to match the same one applied in it ([Dahaghin et al., 2024a](#)).

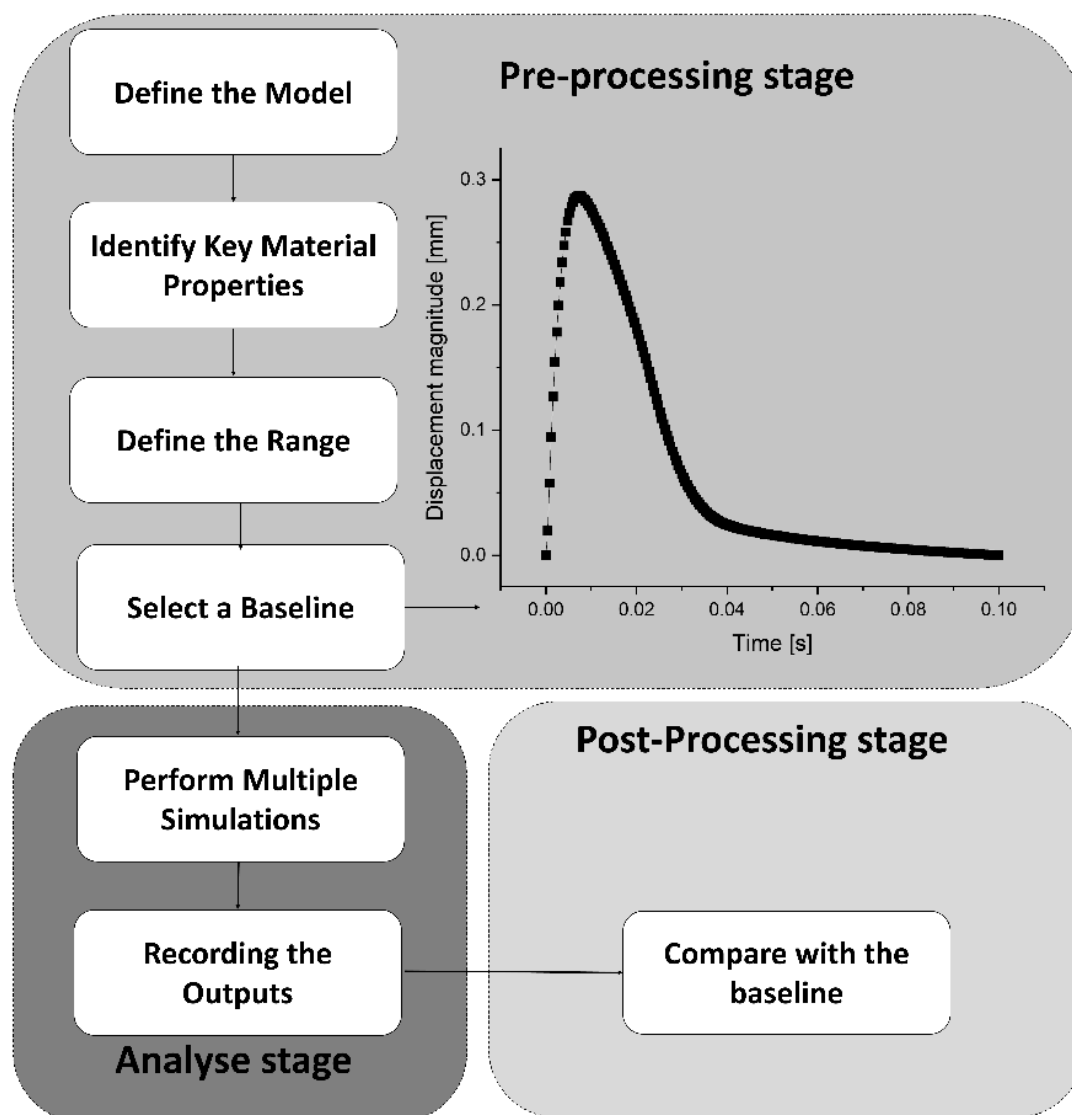
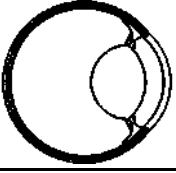



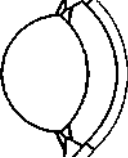


Figure 15. Steps in performing the sensitivity analysis (Dahaghin et al., 2024b).

The process typically begins with a baseline model, which serves as the reference point. To explore the influence of these parameters, we varied Young's modulus across a spectrum ranging from 0.1 to 10 times the baseline value for specific ocular structures. Similarly, we examined Poisson's ratio within a narrow range of values [0.45, 0.46, 0.47, 0.48, and 0.49] (Table 5). Our methodology involved conducting simulations that explored various combinations of Young's modulus and Poisson's ratio values. By systematically varying these parameters and observing their effects on the crystalline lens displacement, we aimed to modify the input variables and observe resulting changes in the model performance.

Table 5. Material properties of the porcine eye (The baseline values are highlighted in grey) ([Dahaghin et al., 2024a](#)).

Modelled parts	Density [kg/m ³]	Young's modulus [MPa]	Poisson's ratio [-]
Sclera 	1400	0.1 $E_s=2.8$	$\nu_s=0.45$
		0.5 $E_s=1.4$	$\nu_s=0.46$
		$E_s=28.0$	$\nu_s=0.47$
		2 $E_s=56.0$	$\nu_s=0.48$
		10 $E_s=280.0$	$\nu_s=0.49$
Cornea 	1400	0.1 $E_c=1.2$	$\nu_c=0.45$
		0.5 $E_c=6.0$	$\nu_c=0.46$
		$E_c=12.0$	$\nu_c=0.47$
		2 $E_c=24.0$	$\nu_c=0.48$
Muscle 	1600	0.1 $E_m=1.1$	$\nu_m=0.45$
		0.5 $E_m=5.5$	$\nu_m=0.46$
		$E_m=11.0$	$\nu_m=0.47$
		2 $E_m=22.0$	$\nu_m=0.48$
Lens 	1100	0.1 $E_l=0.15$	$\nu_l=0.45$
		0.5 $E_l=0.75$	$\nu_l=0.46$
		$E_l=1.50$	$\nu_l=0.47$
		2 $E_l=3.00$	$\nu_l=0.48$
Zonule fibers 	1000	0.1 $E_z=0.095$	$\nu_z=0.45$
		0.5 $E_z=0.475$	$\nu_z=0.46$
		$E_z=0.950$	$\nu_z=0.47$
		2 $E_z=1.900$	$\nu_z=0.48$
		10 $E_z=9.500$	$\nu_z=0.49$

As shown in Figure 16, to quantify the overshooting data of the crystalline lens apex, we defined several parameters:

- the magnitude of the maximum displacement (D_{max}),
- the time when this maximum displacement occurs (t_{peak}),
- the duration until stabilization ($t_{balance}$), which signifies when the lens returns to 10% of its total displacement.

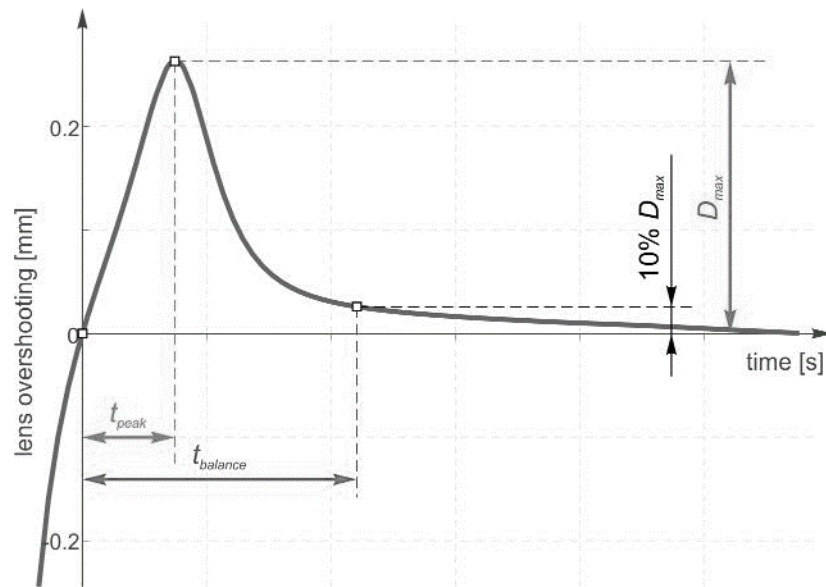


Figure 16. Quantified parameters of the crystalline lens apex displacement (sourced from the submitted manuscripts).

4.4 Results

4.4.1 Young's Modulus

The exploration of biomechanical responses in the crystalline lens across all elastic modulus (E) values has provided a delicate understanding of the mechanical behavior of the ocular system under varying conditions. This comparative analysis was facilitated by examining following Figures which visually represent the percentage differences in the parameters under all consideration. These figures display the comparative biomechanical effects of various eye components (e.g.: cornea, sclera, lens) across a range of E values on crystalline lens overshooting.

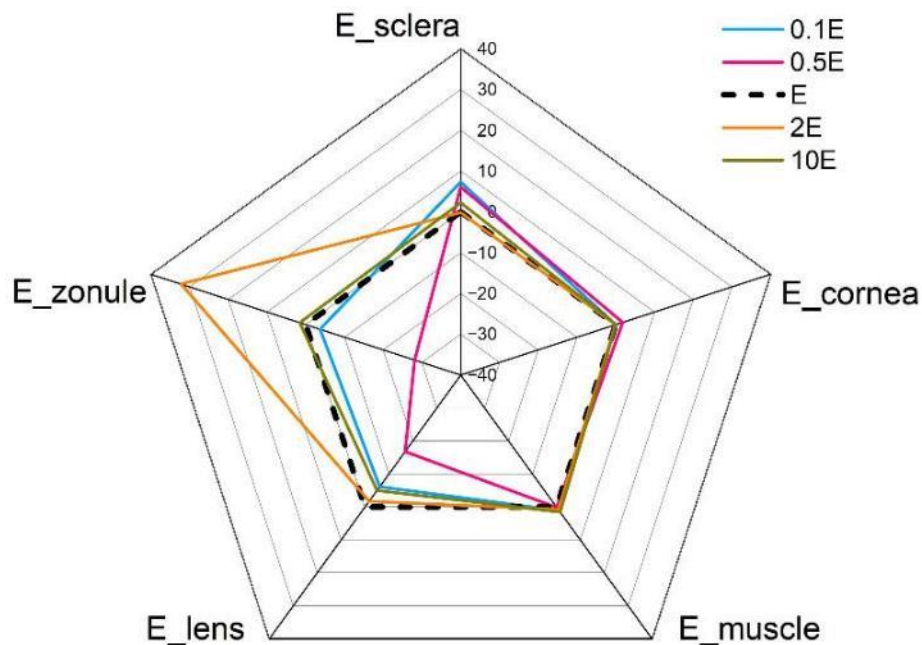


Figure 17. Percentage share of variations in D_{max} for different Young's modulus used in the model components (sourced from the submitted manuscripts).

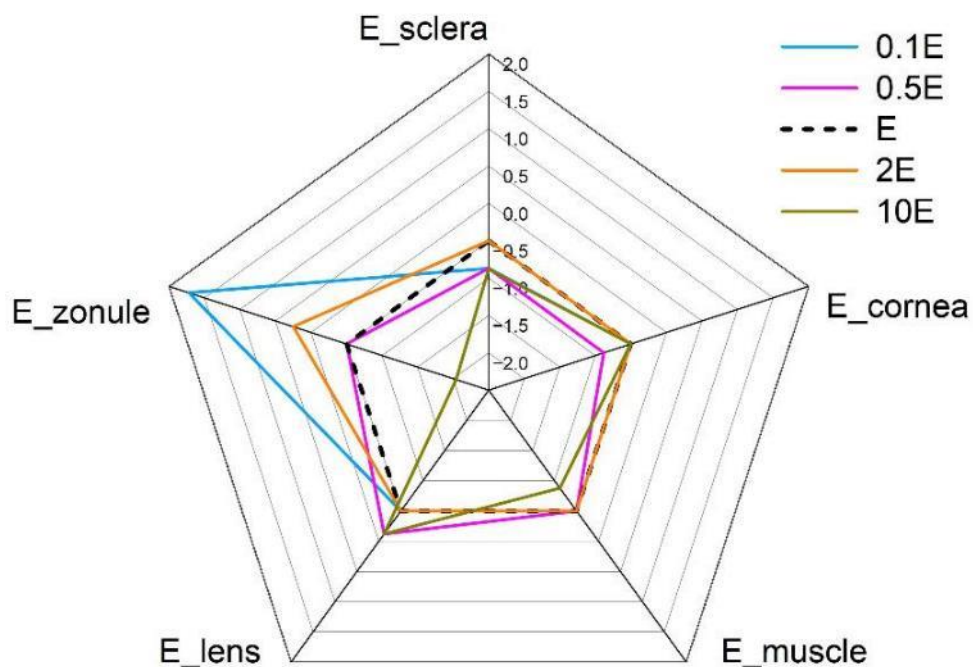


Figure 18. Percentage share of variations in t_{peak} for different Young's modulus used in the model components (sourced from the submitted manuscripts).

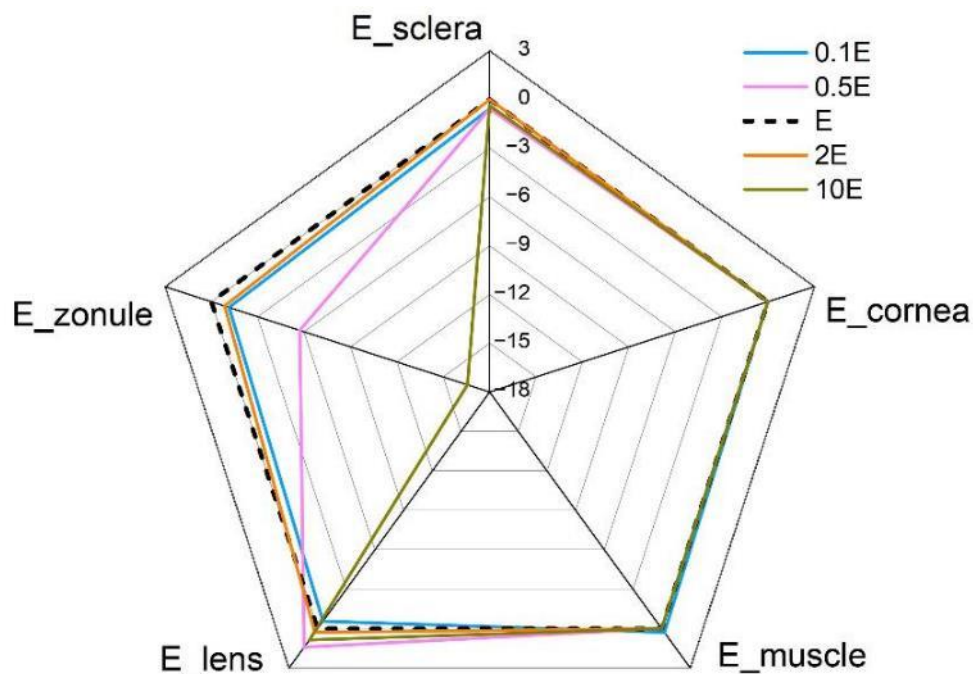


Figure 19. Percentage share of variations in $t_{balance}$ for different Young's modulus used in the model components (sourced from the submitted manuscripts).

Furthermore, beside to spider charts above, Table 6 plays a facilitative role in this analysis by providing a detailed breakdown of the three outcome factors that were quantitatively analyzed. The table presents numerical data that supports the observations made in the figures, allowing for a more precise comparison and interpretation of the results.

The mechanical displacement magnitude graphs in Figure 20 are particularly noteworthy as they offer a visual representation of how the crystalline lens overshoots under the influence of different magnitudes of Young's modulus E . These graphs are instrumental in identifying displacement patterns that may correlate with specific E values, providing a clearer picture of how the elastic modulus affects the mechanical stability of the crystalline lens.

Table 6. Different Young's modulus values and corresponding: D_{max} , t_{peak} and $t_{balance}$ for various tissues (sclera, cornea, muscle, lens, and zonule). Each row involves the alteration of the Young modulus of the specific tissue, while the standard value for the other tissues remains unaltered (sourced from the submitted manuscripts).

Parameter value	0.1·E			0.5·E			E			2·E			10·E		
	D_{max} *	t_{peak} **	$t_{balance}$ ***	D_{max}	t_{peak}	$t_{balance}$	D_{max}	t_{peak}	$t_{balance}$	D_{max}	t_{peak}	$t_{balance}$	D_{max}	t_{peak}	$t_{balance}$
Sclera	0.219	0.105	0.140	0.216	0.105	0.140	0.204	0.106	0.141	0.203	0.106	0.141	0.208	0.105	0.141
Cornea	0.204	0.106	0.141	0.208	0.105	0.141	0.204	0.106	0.141	0.204	0.106	0.141	0.204	0.106	0.141
Muscle	0.206	0.106	0.141	0.204	0.106	0.141	0.204	0.106	0.141	0.206	0.106	0.141	0.207	0.105	0.141
Lens	0.205	0.105	0.139	0.187	0.106	0.142	0.204	0.106	0.141	0.214	0.105	0.140	0.207	0.106	0.141
Zonule	0.196	0.108	0.139	0.159	0.106	0.133	0.204	0.106	0.141	0.300	0.106	0.140	0.207	0.104	0.121

* maximum displacement [mm] ** time of maximum displacement [s] *** stabilization time [s]

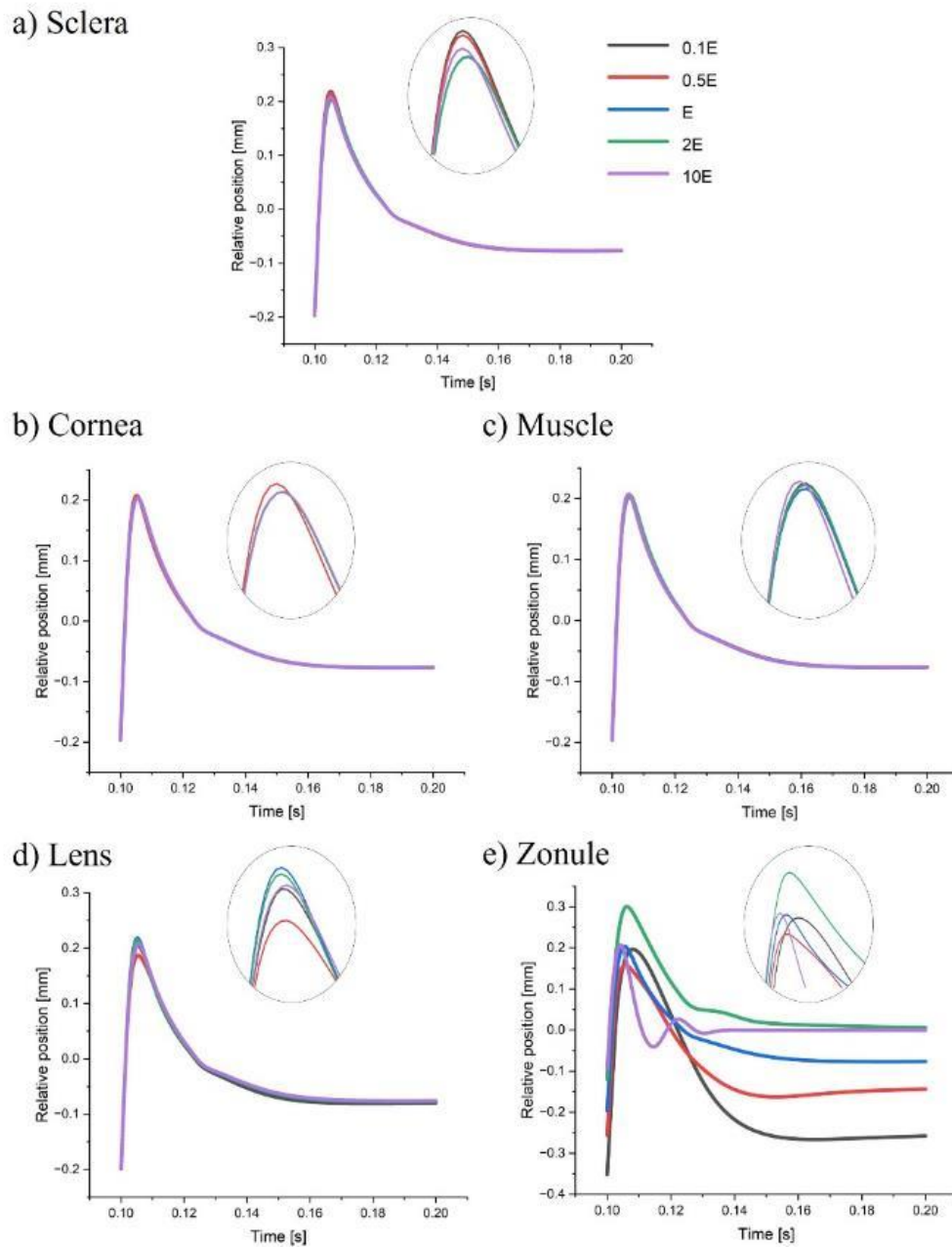


Figure 20. Displacement magnitude in the lens under varying conditions of Young's modulus in different parts of the eye (sourced from the submitted manuscripts).

4.4.2 Poisson's Ratio

The Poisson's ratio plays a crucial role in determining how the lens and its surrounding structures respond to external forces and internal pressures. As a second aim, this research also seeks to evaluate the impact of varying Poisson's ratios on the overshooting parameters. The displacement of the crystalline lens, as illustrated in Figure 21, is clearly the result of the action of the zonules, since no other elements significantly contribute to this phenomenon.

Therefore, the Poisson’s ratio of zonules is a critical factor in altering the displacement of the crystalline lens, and Table 7 presents several key pieces of evidence that support this theory.

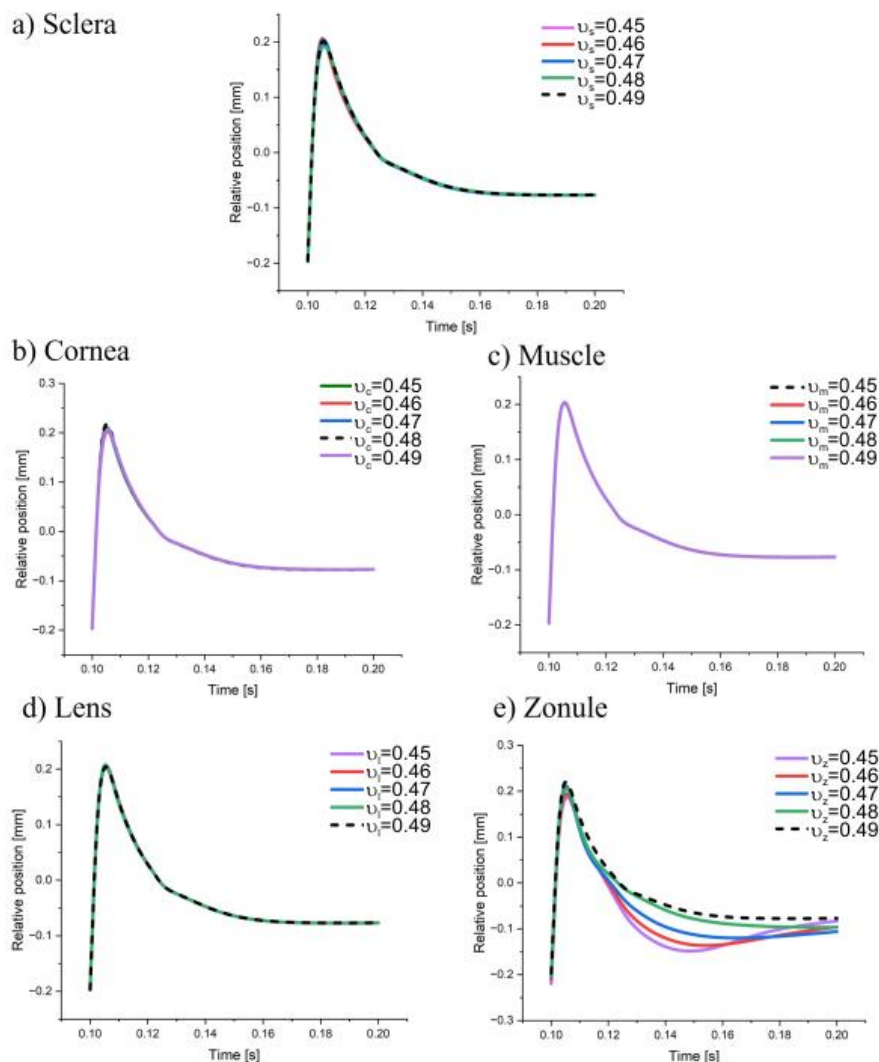


Figure 21. Displacement magnitude in the lens under varying conditions of Poisson’s Ratio in different structures of the eye (sourced from the submitted manuscripts).

Table 7. Different Poisson’s ratio values for the zonular fibers and its corresponding effect on D_{max} , t_{peak} , and $t_{balance}$ (sourced from the submitted manuscripts).

Parameter	$\nu_z=0.45$	$\nu_z=0.46$	$\nu_z=0.47$	$\nu_z=0.48$	$\nu_z=0.49$
D_{max} [mm]	0.187	0.195	0.212	0.206	0.221
t_{peak} [s]	0.106	0.106	0.105	0.106	0.105
$t_{balance}$ [s]	0.124	0.127	0.133	0.143	0.140

As shown in Figure 22, D_{max} is directly influenced by the Poisson’s ratio of the zonules. The study indicates that a decrease in the Poisson’s ratio from 0.49 to 0.45 leads to a varied reduction in D_{max} . This suggests that as the Poisson’s ratio decreases, the zonules become

more compliant, allowing for greater deformation under stress. The range of D_{max} values, from 0.187 to 0.221 mm, highlights the sensitivity of crystalline lens displacement to changes in the material properties of the zonules. This finding is crucial to understanding how alterations in the elastic properties of the zonules, potentially due to aging or disease, can affect lens positioning and, consequently, visual acuity.

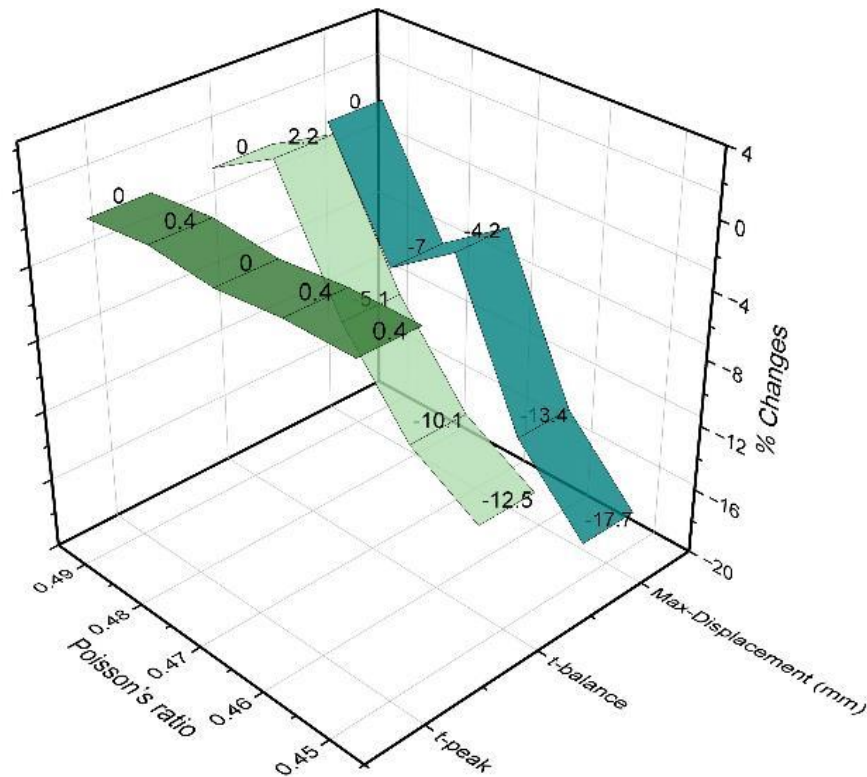


Figure 22. Percentage share of variations in t_{peak} , $t_{balance}$ and D_{max} for different Poisson's ratio values used for zonular fiber (sourced from the submitted manuscripts).

The study also explores the temporal aspects of lens displacement, focusing on t_{peak} and $t_{balance}$. While t_{peak} shows minimal variation across different Poisson's ratios, indicating a consistent temporal response in the initial phase of deformation, $t_{balance}$ is significantly affected by the Poisson's ratio. Lower Poisson's ratios are associated with longer $t_{balance}$ values, suggesting that more compliant zonules require more time to stabilize after deformation. This finding could have implications for the dynamic focusing ability of the eye, known as accommodation, where the speed and efficiency of lens movement are critical for clear vision at varying distances.

4.5 Discussion

As we know, the differences in elasticity and flexibility between living and deceased tissues are significant. Live tissues can deform and return to their original shape, whereas dead tissues become stiffer and lose this ability. An example of this is rigor mortis ([Kori, 2018](#)), the stiffening of muscles after death. In the context of eye tissues, death causes the ciliary body to relax, the zonules to contract, and the lens to thin, similar to the non-accommodative state of the eye.

The results shown in Figure 20 and Figure 21 serve as a starting point for discussing important aspects, such as the role of E_z in the movement of the lens and its effects on eye health. Outputs regarding the displacement of the lens under different levels of E_z , a factor associated with the elasticity of the zonulas, have shown that lower levels lead to a more gradual and smooth displacement, while higher levels result in a faster and more pronounced response. The process unfolds in distinct temporal stages, from an initial phase through mid-phase oscillations to a final steady state, all of which contribute to the overall mechanical behavior. The occurrence of these oscillations is potentially influenced by E_z .

The study also found that the stiffness of the zonules, in terms of Young's modulus, can be a key factor in distinguishing between living and non-living tissues. Below a certain stiffness level, around 2 MPa, the tissue behaves as if it is not alive, losing its elasticity and becoming more damped. This is evident in the lack of oscillation or regular movement in the lens when the tissue is not alive. The results also highlight the importance of the Poisson's ratio of the zonules, suggesting that values below 0.48 lead to unexpected patterns that do not match real-life experiments. The researchers aim to reduce these discrepancies to ensure that their models closely mimic actual eye behavior.

Exploring the impact of Poisson's ratio on the behavior of the zonules has uncovered significant results. The results reveal that changes in D_{max} , t_{peak} , and $t_{balance}$ provide insight into the intricate relationship between the properties of the zonules and the movement of the crystalline lens. A notable observation is that t_{peak} remains constant across varying Poisson's ratios. This implies that the moment of greatest deformation is consistent, regardless of the material characteristics of the zonules. This consistency points to a finely tuned process that governs the timing of zonule reactions during ocular movements, highlighting the intricate nature of the biomechanics involved in eye function.

Conversely, the duration required for the zonules to return to a state of equilibrium ($t_{balance}$) varies, suggesting that the zonules are capable of regaining balance at a faster rate under certain conditions. This swift recovery mechanism may play a vital role in facilitating smooth and efficient eye movements, especially in scenarios where rapid visual adjustments are necessary.

A decrease in the Poisson's ratio, indicating a reduction in the elastic responsiveness of the material, correlates with an increase in the zonular deformation. This suggests that the elasticity of the zonules significantly influences their deformation and, consequently, the movement of the eye. The observed increase in D_{max} may be attributed to changes in the tension and elasticity of the zonular fibers, which could affect how forces are distributed within the eye. These findings enhance our understanding of the mechanical properties of zonules and their contribution to the dynamics of the eye.

4.6 Conclusion

This chapter investigates how changes in material properties affect the crystalline lens overshooting, highlighting the importance of understanding the biomechanics of ocular tissues. It finds that adjusting the stiffness and elasticity of the zonules is key to accurately modeling eye movements. However, the study also points out its shortcomings, such as using *ex vivo* samples and a simplified model, and suggests that future research should include *in vivo* data and explore more complex biomechanical factors.

Chapter 5

In silico Evaluation of the Pressure Effects

5.1 Research Highlights

- 1 IOP is likely to play a crucial role in lens overshooting.
- 2 Regardless of IOP levels, the lens consistently reaches its maximum displacement within a defined time frame, crucial for visual stability.
- 3 Lens overshooting data can be used as a biomarker for IOP estimation.

5.2 Introduction

When the IOP is within its normal range, the lens can flex and change shape with ease, allowing for clear vision at various distances. However, when IOP is elevated or fluctuates significantly, it can lead to biomechanical changes within the eye that may affect the vision. The relationship between IOP and the biomechanical properties of the eye is complex and multifaceted. It involves not only the direct effects of pressure on the lens and other structures but also the indirect effects on the blood flow to the optic nerve and the overall condition of the ocular tissues. Understanding these relationships is crucial for the development of effective treatments for glaucoma and other ocular conditions.

Research into the effects of IOP on lens dynamics could reveal how changes in pressure influence the tension on the zonular fibers, potentially affecting the lens ability to change shape and focus. For example, an increase in IOP could put additional strain on zonular fibers, making it harder for the ciliary muscle to adjust the lens for accommodation.

Biomechanical models that utilize the FEM offer a sophisticated approach to exploring how different configurations influence the eye response to external forces and pressures ([Issarti et al., 2021](#), [Cabeza-Gil et al., 2023](#)). This method is particularly advantageous in the field of ophthalmology, where it can incorporate various parameters such as IOP. In their studies, Salimi et al. have highlighted the importance of IOP fluctuations and their impact on the eye ([Salimi et al., 2011](#)). They have demonstrated that changes in IOP can alter the natural frequencies at which the lens vibrates, as well as its overall vibrational characteristics. This is a critical finding, as it suggests that the mechanical stability of the lens is directly influenced by the pressure within the eye.

This chapter investigates the impact of IOP on the oscillatory behavior of the crystalline lens in an *ex vivo* context. By manipulating IOP within a porcine eye model, which was previously developed and validated in Chapter 3, and employing sophisticated fluid-structure interaction (FSI) methodologies, the study aims to precisely measure lens overshooting under specific conditions. The findings from this study are expected to have direct clinical relevance, potentially leading to the development of a novel, non-invasive approach to measuring IOP.

5.3 Variation in intraocular pressure

In the current chapter, I am going to delve into the intricate dynamics of the ocular system by employing the first optomechanical eye model that has been validated ([Dahaghin et al., 2024a](#)) and is utilized to scrutinize the mechanical responses of a porcine eye when subjected to varying levels of IOP. This model incorporates the complex interactions between the fluids within the eye and its structural components through the application of fluid-structure interaction (FSI) principles. The FSI approach allows us to simulate the intricate mechanical interplay between the ocular fluids and the solid structures of the eye, providing a comprehensive understanding of the behavior under physiological conditions.

The vitreous body and the aqueous humor, which are critical components of the ocular fluids, are modeled as viscous Newtonian fluids that are incompressible. This choice of modeling is based on the premise that these fluids exhibit a linear relationship between stress and strain rate, a characteristic that is essential for accurately capturing their dynamic behavior. The dynamic viscosity of these fluids is set to 0.00074 Pa·s, and a density of 1000 kg/m³ is assigned to ensure that the model faithfully represents the physical properties of the ocular fluids ([Singh et al., 2017](#)). These parameters are crucial for simulating the fluid dynamics within the eye accurately.

The role of the ocular fluids in the model is pivotal, as they are directly responsible for the transmission of pressure throughout the eye, thereby influencing the IOP. To investigate the effects of IOP on the mechanical behavior, we applied a series of IOP values ranging from 15 to 20 mmHg, with a total of six distinct pressure levels being tested. This approach allows us to systematically analyze the eye response to a spectrum of physiologically relevant pressures.

It is important to note that while the IOP was varied across the different models, the material properties and boundary conditions for the solid parts of the eye were held constant. This consistency ensures that any observed variations in the mechanical behavior of the eye can be attributed solely to changes in IOP.

The apex point of the crystalline lens, highlighted in Figure 23 with red points, plays a crucial role in this analysis. This specific point is strategically chosen as the reference point for exact tracking and quantifying the mechanical displacement of the crystalline lens. The selection of this point is not arbitrary. This point is chosen because it represents a key anatomical landmark that is easily identifiable and closely associated with the optical axis

of the eye. By focusing on this specific location, we can obtain precise measurements that are directly relevant to the optical function of the eye.

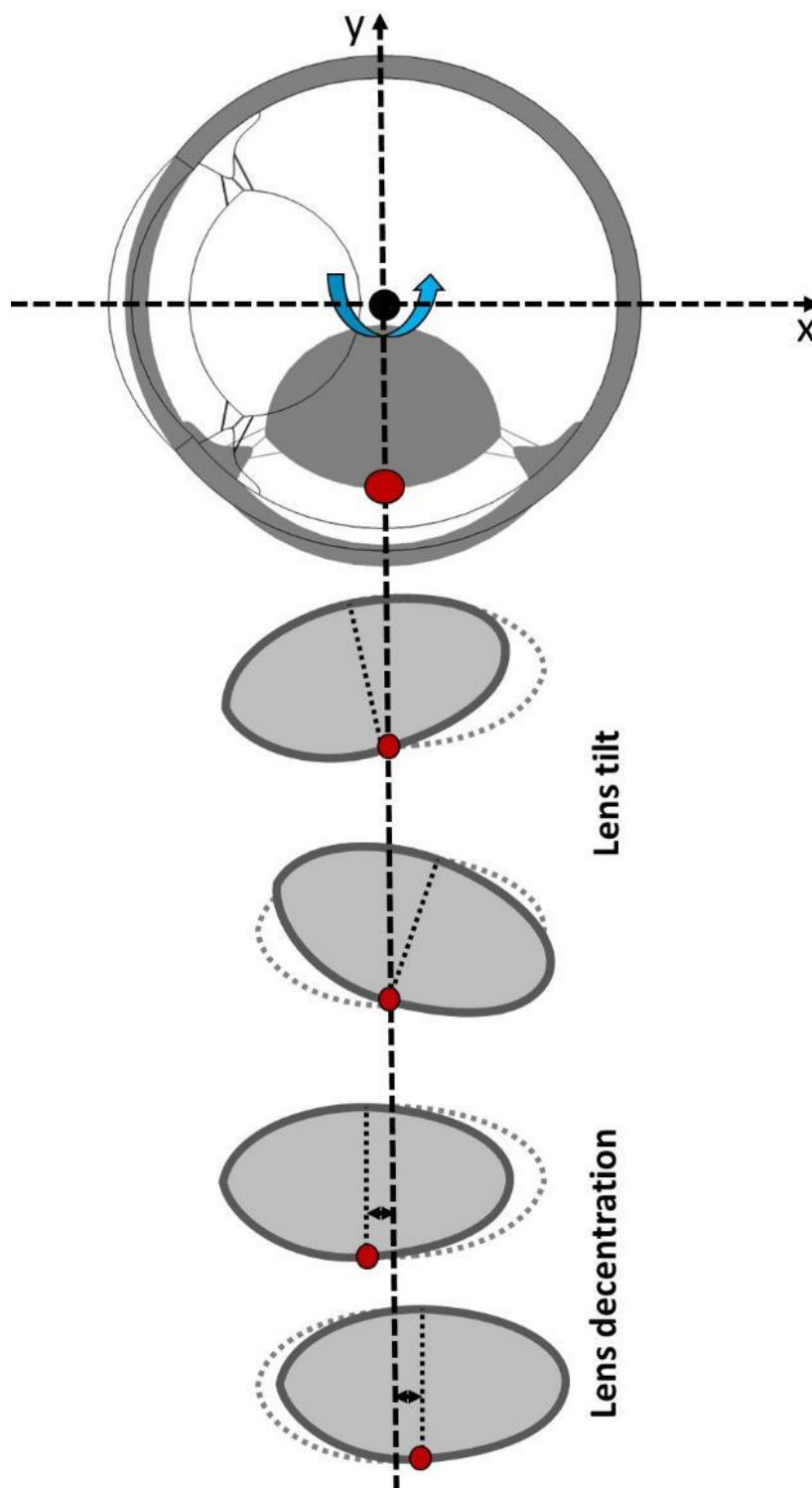


Figure 23. Illustration of decentration and tilt of the crystalline lens being induced by rotation motion of the whole eye globe (sourced from the submitted manuscripts).

This displacement includes two primary aspects: the tilt and the decentration of the lens. The tilt of the crystalline lens refers to the angular deviation of the lens from its normal, aligned position within the eye. Decentration, on the other hand, involves the lateral displacement of the lens from its central position.

5.4 Results

The outputs in Figure 24 provide a clear insight into the relationship between IOP and D_{max} . This inverse correlation is not only statistically significant but also has important implications for biomechanics of the eye.

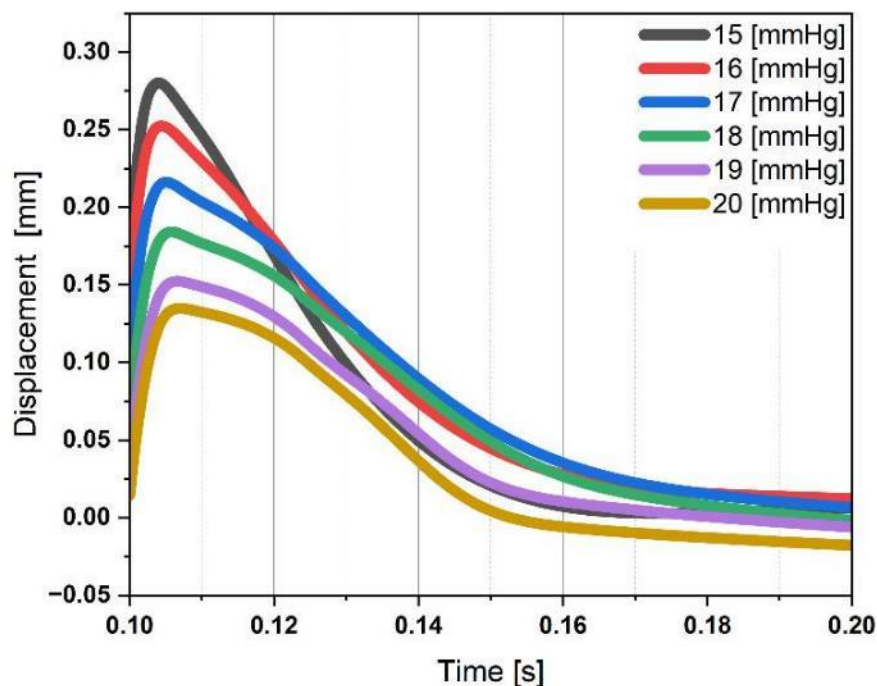


Figure 24. Time evolution of apex position of the crystalline lens during overshooting (sourced from the submitted manuscripts).

As the data show, when the IOP is at a lower level, such as 15 mmHg, the lens exhibits a greater degree of movement, with a D_{max} of 0.280 mm. This level of displacement suggests that the lens is able to move with relative ease in response to the forces exerted during sudden stops or rapid changes in direction. This unimpeded movement is crucial for the proper functioning of the accommodation system, which is responsible for focusing on objects at different distances.

However, as the IOP increases to 20 mmHg, the lens ability to move is significantly reduced, with D_{max} decreasing to 0.135 mm. This reduction in displacement indicates that the higher IOP levels are creating increased resistance within the eye, making it more difficult for the lens to change position. This increased resistance could potentially impair the eye's ability to accommodate, leading to a reduction in visual performance, particularly in tasks that require frequent or rapid changes in focus.

When IOP is increased, the lens's capacity to move is compromised. the decrease in D_{max} , is indicative of the reduced range of motion that the lens experiences under higher IOP. The relationship between IOP and the mechanical properties of the eye is complex and multifaceted. The resistance to lens displacement is not only influenced by the direct pressure exerted on the lens but also by the surrounding structures, such as the ciliary muscle and the zonular fibers that connect the lens to the ciliary body. These structures must work against the increased IOP to allow for lens movement, and their ability to do so is diminished as pressure rises.

The data presented in Table 8 provides evidence for the theory that IOP has a direct effect on the kinematics of the lens, specifically its velocity and acceleration during overshooting. The reduction in velocity and acceleration with increasing IOP suggests that the lens dynamic response is dampened, which could lead to faster and more precise focusing.

Table 8. The maximum velocity and acceleration data of the apex position of the crystalline lens during overshooting for all IOP levels (sourced from the submitted manuscripts).

IOP	[mmHg]	15	16	17	18	19	20
Velocity	[$\mu\text{m}/\text{ms}$]	22.2	19.2	13.5	10.4	8.4	7.5
Acceleration	[$\mu\text{m}/\text{ms}^2$]	56.4	49.6	42.3	37.9	34.6	31.8

The stability of t_{peak} (0.104 to 0.107 seconds) across varying IOPs indicates a strength in the lens's ability to achieve its D_{max} within a narrow temporal period. This consistency may be attributed to the structural integrity of the ocular components that support it. The lens' behavior in reaching D_{max} within a specific timeframe suggests a potential biological optimization for rapid accommodation to changes in IOP under different physiological conditions.

On the other hand, the observed variability in $t_{balance}$, ranging from 0.154 to 0.188 seconds, across different IOPs may reflect the complex interplay of factors involved in the lens's return to its baseline state. This could include the viscoelastic properties of the lens and surrounding tissues, the role of ciliary muscle activity, and the influence of vitreous humor dynamics. The slight differences in $t_{balance}$ could also be indicative of the body's adaptive mechanisms to counteract the effects of varying IOPs, ensuring that the lens can stabilize and resume its normal function efficiently.

Table 9 in detail outlines the comprehensive variations in the measured parameters as a percentage of changes from the standard pressure of 15 mmHg. This detailed analysis allows for a clear understanding of how these parameters deviate from the established baseline, offering insights into the behavior of the system under varying conditions. The table serves as a valuable reference for identifying trends and patterns in the data, facilitating a deeper comprehension of the model's response to changes in pressure.

Table 9. Overshooting parameters for the six IOP levels and their relative variation with respect to the initial level of 15 mmHg (sourced from the submitted manuscripts).

IOP [mmHg]	15	16	17	18	19	20
t_{peak} [s]	0.104	0.1044	0.1052	0.1056	0.1064	0.1068
		0.4 %	1.2 %	1.5 %	2.3 %	2.7 %
$t_{balance}$ [s]	0.154	0.170	0.185	0.188	0.186	0.181
		10.7 %	20.3 %	22.1 %	20.8 %	18.0 %
D_{max} [mm]	0.280	0.252	0.216	0.184	0.152	0.135
		-9.9 %	-22.9 %	-34.3 %	-45.7 %	-51.9 %

Figure 25 extends our understanding by providing graphical details of the relationship between IOP and the mechanical behavior of the lens within the eye. By manipulating the IOP levels in the simulations, we observe a spectrum of responses that highlight the sensitivity of lens displacement to this critical physiological parameter. The disparities in crystalline lens displacement magnitude and duration across varying IOP levels indicate that the mechanical interaction between the lens and its surrounding structures seems to be dynamic and pressure-dependent.

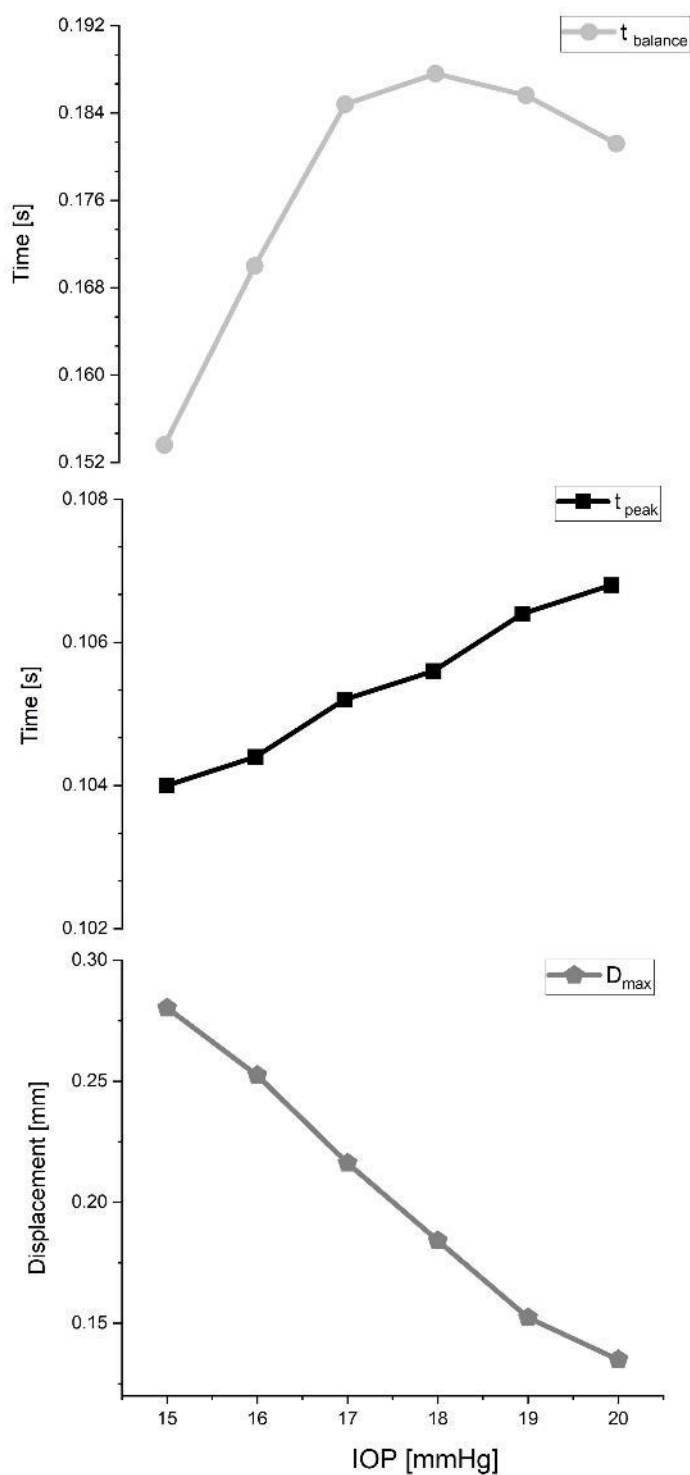


Figure 25. The trend of observed changes in $t_{balance}$, t_{peak} and D_{max} , with increasing IOP levels (sourced from the submitted manuscripts).

By further analyzing the data presented in the spider chart (Figure 26), we were able to figure out complex relationships between IOP fluctuations and the subsequent displacement of the lens. The chart's radial axes allowed us to visualize multiple variables simultaneously, revealing that as IOP levels increased, the lens exhibited not only greater displacement but also an extended duration of movement before stabilizing. This phenomenon

was particularly notable at higher IOP levels, suggesting a linear relationship between IOP and lens dynamics.

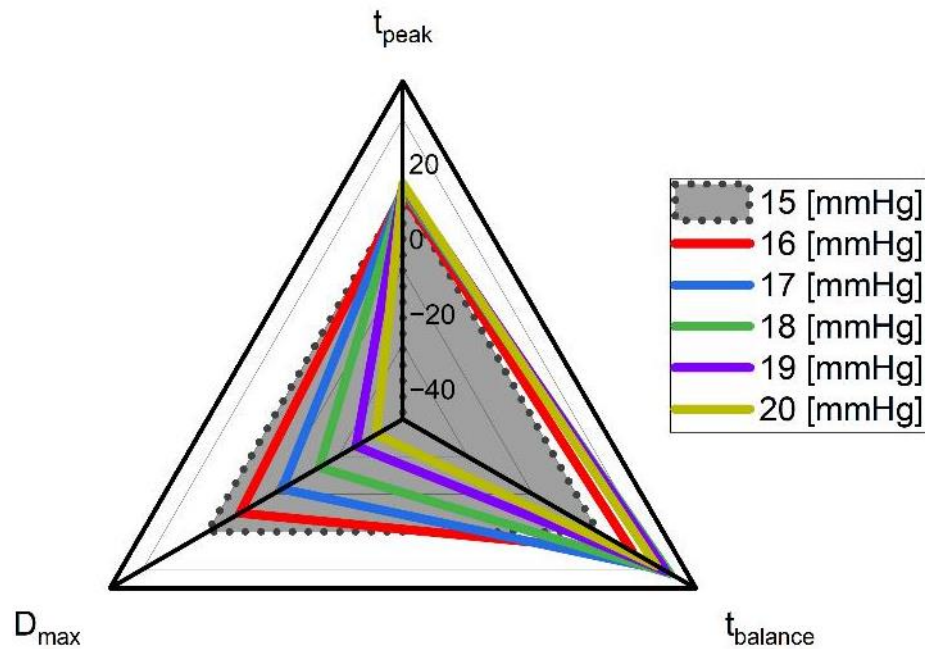


Figure 26. Analyzing trends based on the percentage change in lens displacement patterns across various levels of intraocular pressure (sourced from the submitted manuscripts).

5.5 Discussion

The biomechanical response of the eye to sudden movements, such as rapid head turns, involves a complex interplay of forces that can transiently alter IOP. The lens, being a key component of the eye's optical system, plays a significant role in this dynamic response due to its mechanical properties and position within the eye. The observed inverse relationship between IOP and D_{max} during sudden stops suggests that as IOP increases, the mobility of the lens decreases, leading to a reduction in D_{max} . This phenomenon can be attributed to the increased resistance within the eye's internal environment, which opposes the forces acting on the lens. Consequently, the lens exhibits less movement, indicating that the structural integrity is more effectively maintained against external forces at higher IOP levels.

The consistent nature of the t_{peak} , irrespective of variations in IOP, underscores the robustness and precision of the lens's response. This phenomenon highlights a sophisticated mechanical system within the eye that ensures a rapid yet controlled displacement of the lens in response to sudden decelerations.

In contrast, the observed variation in $t_{balance}$ suggests that factors beyond IOP play a role in lens stabilization. These may include the elasticity of the lens itself and the biomechanical characteristics of the surrounding ocular structures ([Van Alphen and Graebel, 1991](#)). The lens, as a key component of this system, must be able to adapt to changes in its environment, such as fluctuations in IOP, while maintaining its ability to focus light onto the retina. The extended time of lens movement under high IOP conditions could potentially lead to transient visual disturbances or even long-term changes in lens position, which could affect vision quality.

5.6 Conclusion

This chapter offers significant insights into the crystalline lens reaction to fluctuations in IOP by utilizing porcine eyes as a model. Through finite element analysis, we observed unique patterns of lens displacement in response to varying IOP levels. The implications of these findings are profound for both clinical practice and research in ocular biomechanics, suggesting potential advancements in diagnostic tools.

Chapter 6

In silico Reconstruction of *In vivo* Experiment

6.1 Research Highlights

- 1 Exploring the relationship between IOP and Crystalline Lens dynamics, offering a new perspective on ocular health.
- 2 Investigating the mechanics of lens wobbling through optomechanical simulations.
- 3 Developing an innovative approach to IOP measurement, aimed at enhancing both patient comfort and accuracy.

6.2 Introduction

The *in vivo* FEM models in the study of ocular issues is well-recognized among ophthalmologists, including the interactions between fluids and ocular structures ([Redaelli et al., 2022](#)), the effects of intraocular pressure ([Dai et al., 2017](#)), and the accommodative process ([Cabeza - Gil et al., 2021](#)). Despite the significant focus on static lens modeling in the literature, there is a noticeable lack of emphasis on dynamic aspects, such as changes in gaze, which presents a significant gap.

This chapter aims to advance our knowledge of the crystalline lens's dynamic behavior by modeling the relationship between IOP and lens wobbling, a topic of increasing importance due to its potential implications in ocular mechanics. Despite the lack of literature on realistic visualizations of lens wobbling using combined mechanical and optical finite element method investigations, this chapter seeks to capture and analyze lens wobbling at different IOP levels through the optomechanical simulations. The outcomes are anticipated to offer significant contributions to the understanding of IOP-wobbling correlations, ultimately aiming to facilitate the creation of novel IOP measurement techniques and improve diagnostic accuracy in ophthalmology.

6.3 Materials and Methods

The research methodology, motivated by the Purkinje image behavior under varying IOP induced by a water drinking test protocol (WDT), conducted by the Visual Optics Group, as depicted in Figure 10. FEM was employed to investigate the wobbling and the time required for stabilization. The simulation results were then used as parameters for the subsequent optical simulations. Finally, the optomechanical simulation outcomes were compared with experimental data for validation purposes (Figure 27).

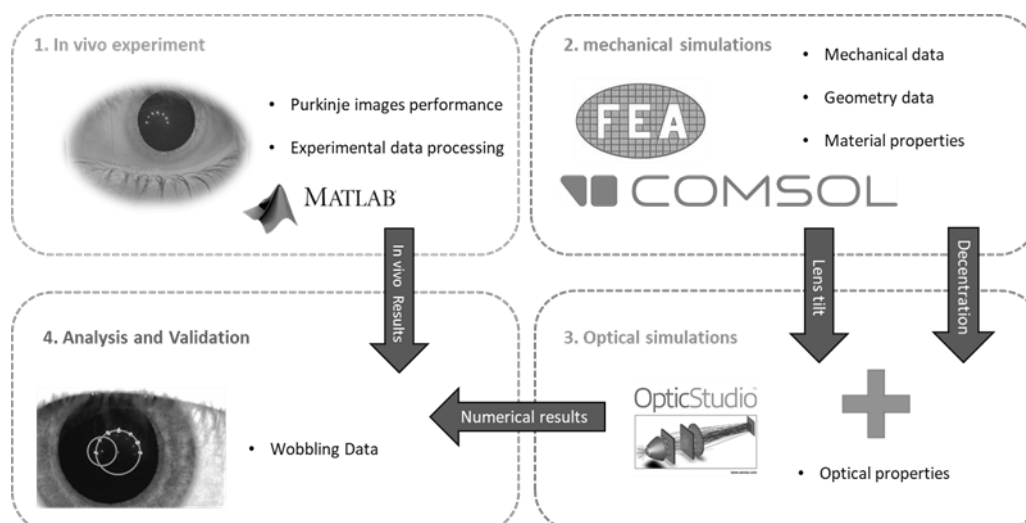


Figure 27. Steps involved in the study and simulation process. The diagram outlines the key stages and their interconnections, providing a visual guide to the overall workflow (sourced from the submitted manuscripts).

6.3.1.1 Mechanical Simulations

In the mechanical simulation, a simplified model of the human eye was constructed using COMSOL Multiphysics, which included the cornea, sclera, ciliary body, aqueous humor, lens, and vitreous. The model, as depicted in Figure 28, has an overall length of 24 mm for the eye globe, with the cornea's apex thickness being 0.57 mm. The anterior chamber depth is estimated at 2.99 mm, the lens thickness is 3.52 mm, the vitreous length is about 16 mm, and the sclera's thickness is set at 0.76 mm. The capsule has a uniform thickness of 0.1 mm. These geometric parameters are based on the accommodation and age-dependent eye model for a 20-year-old eye with the state of accommodation of 2.5 diopters. Additional dimensional details are provided in Table 10, which are based on literature data ([Dai et al., 2017](#), [Cabeza - Gil et al., 2021](#), [Zapata-Díaz et al., 2019](#)).

Table 10. Summary of geometrical parameters.

Modelled Parameters	Radius [mm]	Asphericity
Anterior corneal surface	7.87	-0.18
Posterior corneal surface	6.40	-0.12
Anterior lens surface	9.825	-7.05
Posterior lens surface	5.649	-4.6
Inner sclera surface	10.81	0.193
Outer sclera surface	11.58	0.193.
Anterior nucleus surface*	4.5	n.a.
Posterior nucleus surface*	4	n.a.

*The nucleus of the lens was included only for the mechanical simulations.

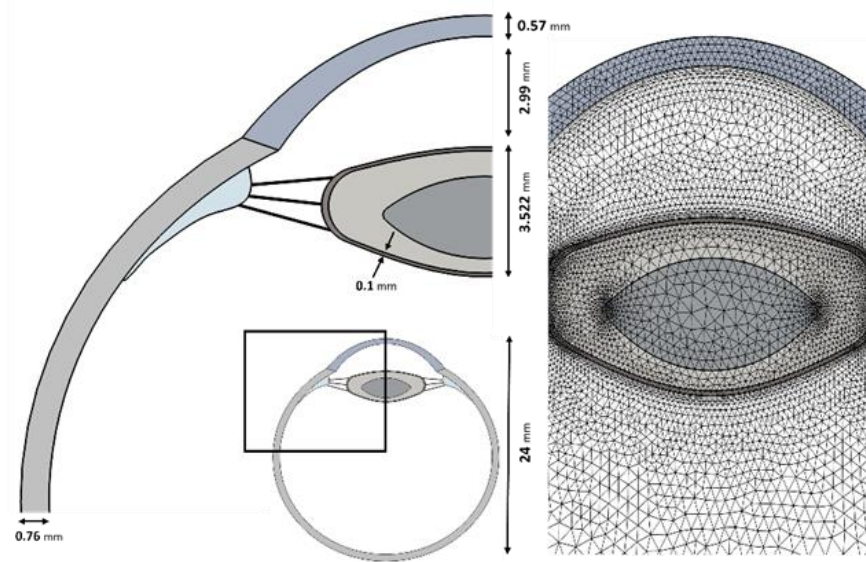


Figure 28. Geometry of the model containing the main and the most influential elements in eye biomechanics: lens, capsular bag, vitreous body, zonular fibers, cornea, sclera, aqueous humour and ciliary muscle (sourced from the submitted manuscripts).

To accurately understand the mechanical behavior of the human eye, it is crucial to meticulously choose material properties that align with those reported in scientific literature. The specific values for Young's modulus, Poisson's ratio, and density for each component of the eye are detailed in Table 11, based on references.

Table 11. Mechanical Properties Assigned to Ocular Tissues ([Issarti et al., 2021](#), [Cabeza - Gil et al., 2021](#), [Osmers et al., 2021](#), [Bocskai and Bojtár, 2013](#)).

Tissues	Young's modulus [kPa]	Poisson's ratio [-]	Density [kg/m ³]
Cornea	400	0.42	1400
Capsule	1000	0.49	1078
Crystalline lens	Cortex	3	1078
	Nucleus	0.3	1078
Sclera	3000	0.47	1400
Ciliary Muscle	350	0.47	1225
Zonular Fibers	1500	0.49	1000

Both the vitreous body and aqueous humor were modeled as viscous Newtonian incompressible fluid, With a density of $1,000 \text{ kg/m}^3$ and a dynamic viscosity of $0.00074 \text{ Pa}\cdot\text{s}$, subjected to series of pressure values , which played the role of the IOP in the model.

A detailed check using a special measure called "equiangular skew" has been implemented to carefully assessment the quality of element. This check provides a score from 0 to 1, with anything over 0.5 considered good enough (Etminan et al., 2023). This model used 44,522 triangles elements with an average quality score of 0.82, which is excellent for analyzing complex shapes.

The eyeball was modeled to rotate around an axis positioned 13.19 mm behind the apex of the cornea, near the center of the eye. This axis allows for a 10 degree rotation around the vertical axis perpendicular to the 2D model. The rotation profile followed an angular velocity of up to 320 deg/s , based on data available in the literature (Martin et al., 2009). Aside from the specified rotation parameters, all other governing equations and boundary conditions were set to closely mimic the conditions of the *ex vivo* study (Dahaghin et al., 2024a).

6.3.1.2 Optical Simulations

In the optical part, a comprehensive model of the eye, complete with an illumination system and Purkinje reflection imaging, was developed using Zemax OpticStudio software in non-sequential mode. The model's specifications, as detailed in reference (Boszczyk et al., 2023), were adjusted to incorporate the parameters of an accommodated eye. The refractive indices used in the model are presented in Table 12.

Table 12. Summary of optical parameters.

Modelled Parameters	Refractive index
Anterior corneal surface	1.376
Posterior corneal surface	1.336
Anterior lens surface	1.4332
Posterior lens surface	1.336

The output data from mechanical simulations, which tracked the x and y coordinate changes of each eye surface over time, served as the input for the optical simulations. The relationship between the $PIV-PI$ and the position of the lens took a form:

$$PIV - PI = 0.04147 \text{ tilt} - 1.059 \text{ dec} - 0.003, \quad (11)$$

6.4 Results

The analysis of the data collected from the study subjects under controlled IOP conditions has revealed a spectrum of individual responses that are both intriguing and significant for understanding the mechanics of the eye. The unique wobbling patterns observed in each subject suggest that the eye's lens movement is not a uniform process but rather a highly individualized one, influenced by a variety of factors (Figure 9).

A crystalline lens wobbling pattern looks like a decaying sinusoidal wave, representing the oscillations of the system gradually decreasing in amplitude over time, can be successfully described by a harmonic oscillator characteristics. The parameters frequency, *Q-factor*, and damping ratio were estimated through a spectral analysis of a wobbling pattern. The frequency represents how fast the system oscillates or wobbles. In spectral analysis, frequency is determined by identifying the dominant peaks in the frequency spectrum of the wobbling pattern. The *Q-factor* measures how underdamped an oscillation or resonator is. It is defined as the ratio of the center frequency to the 3dB bandwidth of the spectrum. The damping ratio describes how oscillations decay over time. It is related to the *Q-factor* and indicates how quickly the system returns to equilibrium after being disturbed. A lower damping ratio means the system oscillates for longer, while a higher damping ratio suggests the oscillations die out more quickly.

The range of frequencies observed, from 18.45 to 33.78 Hz, underlines the dynamic nature of the lens movement under normal physiological conditions. This wide range indicates that the lens can exhibit a variety of oscillatory behaviors, which may be influenced by factors such as the elasticity of the lens capsule, the viscosity of the vitreous humor, and the tension of the zonular fibers.

The *Q-factors*, which provide insight into the degree of damping in the oscillatory system of the lens, varied significantly among subjects, from 1.11 to 2.37. This variation suggests that there is a range of damping behaviors within the normal population, which could be due to differences in the biomechanical properties of the components. According to the classification of *Q-factors*, a system with a *Q-factor* $>1/2$ is considered underdamped, meaning it exhibits oscillations with a decaying amplitude. Therefore, all the measured *Q-factors* suggest that the lens oscillations in these subjects were underdamped. The damping ratio, which further characterizes the decay of oscillations in the lens, ranged from 0.21

to 0.45. Finally, D_{max} observed, ranging from 0.16 to 0.72 mm, highlight the significant variation in the amplitude of lens movement among individuals.

Following the water drinking test, there was a marked decrease in crystalline lens wobbling as depicted in Figure 10 along with considerable changes in parameters as shown in Table 13.

Table 13. Wobbling data (sourced from the submitted manuscripts).

Subject No.	condition	Frequency [Hz]	Q -factor	Damping ratio	D_{max} [mm]
S#1	Physiological	22.21	1.17	0.42	0.45
	WDT	21.20	1.31	0.38	0.52
S#2	Physiological	24.36	2.37	0.21	0.26
	WDT	23.86	2.71	0.19	0.17
S#3	Physiological	25.57	1.29	0.39	0.16
	WDT	28.35	1.16	0.43	0.14
S#4	Physiological	21.13	1.81	0.27	0.72
	WDT	18.38	1.74	0.29	0.58
S#5	Physiological	33.78	1.11	0.45	0.16
	WDT	27.95	1.03	0.48	0.12
S#6	Physiological	18.45	2.00	0.25	0.24
	WDT	25.38	1.53	0.33	0.14

The data presented in Figure 29 reveals a consistent pattern in the average frequency across different subjects. Notably, there is a consistent rise in damping ratios post-WDT. Furthermore, there is a general decline in D_{max} values and Q -factors also follow this trend.

In a similar path to the experimental findings, the simulations also elucidate a coherent and reproducible trend of oscillations within the crystalline lens, as depicted in Figure 30. As IOP levels are progressively raised, the simulations indicate methodical and predictable alterations in certain parameters associated with the displacement of the lens.

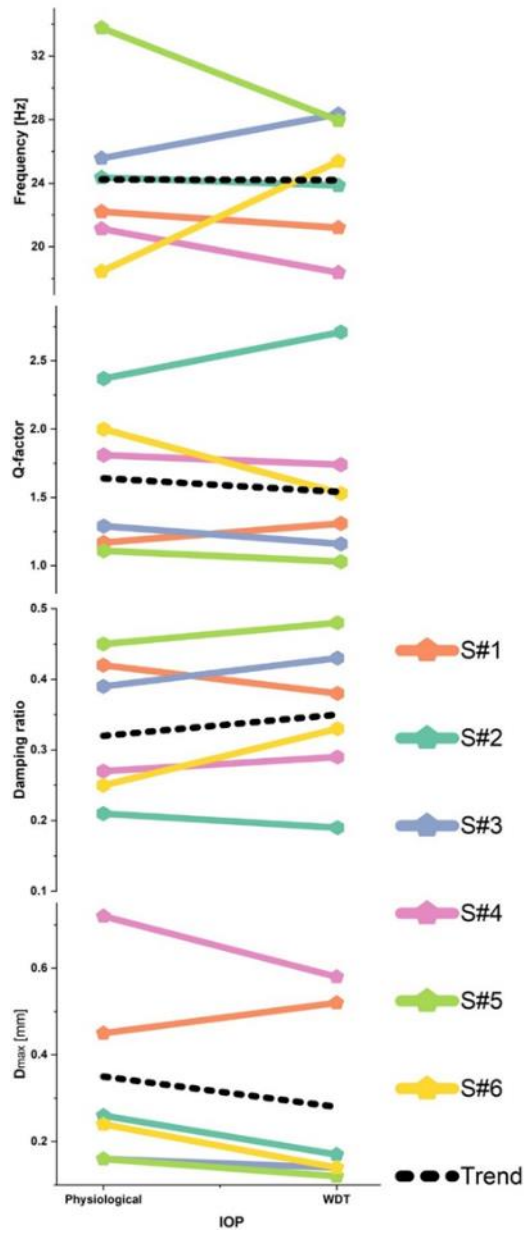


Figure 29. Analysed parameters for WDT results (sourced from the submitted manuscripts).

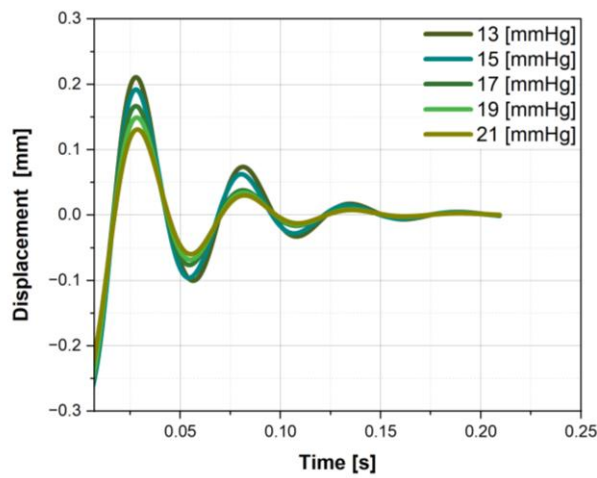


Figure 30. Simulation pattern for all IOP levels (sourced from the submitted manuscripts).

In Table 14, at a minimal IOP of 13 mmHg, the frequency was precisely measured at 19.46 Hz. This measurement was taken alongside a corresponding Q -factor with a value of 2.25, and the damping ratio was computed to be 0.22. D_{\max} at this pressure level was recorded as 0.22 mm, which measures the amplitude of the oscillations of the lens. This value is significant as it provides information about the physical movement of the lens.

Table 14. Simulation data for all IOP levels (sourced from the submitted manuscripts).

IOP [mmHg]	Frequency [Hz]	Q-factor	Damping ratio	D_{\max} [mm]
13	19	2.25	0.22	0.22
15	19	2.17	0.23	0.20
17	19	1.96	0.25	0.17
19	19	1.94	0.26	0.15
21	19	1.82	0.27	0.13

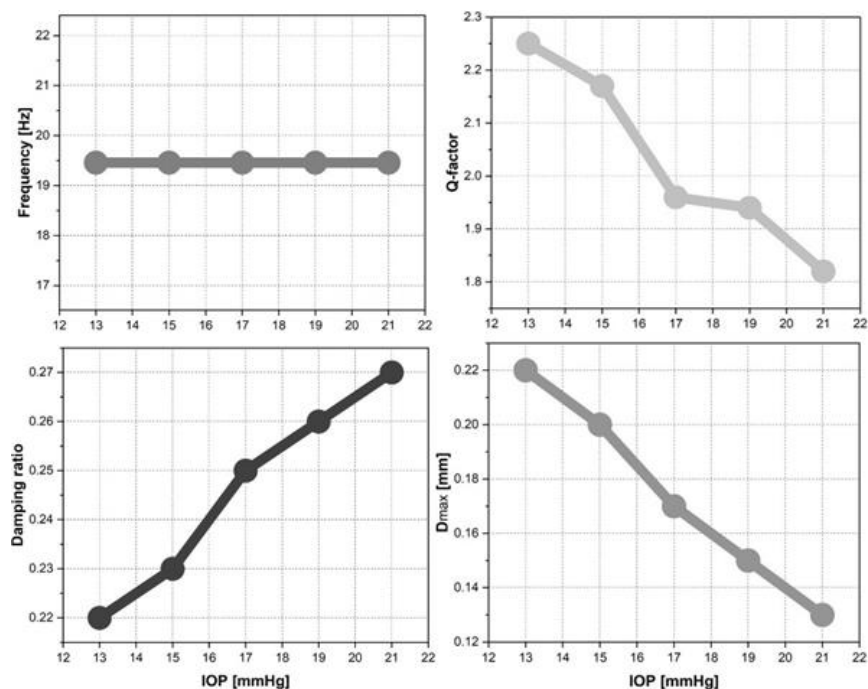


Figure 31. Analysed parameters for simulation results (sourced from the submitted manuscripts).

For higher levels of IOP, the frequency remained relatively constant at approximately 19 Hz across all levels. This consistency in frequency suggests that the IOP does not significantly affect the rate at which the lens oscillates within the tested range. However, alterations were noted in other parameters as the IOP increased. For example,

with an increase in IOP, the D_{\max} value exhibits a clear downward trend (Figure 31), dropping from 0.21 mm at 13 mmHg to 0.13 mm at 21 mmHg.

6.5 Discussion

The WDT results, shown in Figure 10, demonstrate that wobbling decreases with increased IOP, but the rate of decrease varies, suggesting that the impact of IOP on the onset of glaucoma ([Susanna et al., 2005](#)) may differ among subjects. This variability may be more closely related to the mechanical properties of the aqueous humor and vitreous body than to other ocular structures, with implications for the control and stability of lens movement ([Eppig et al., 2013](#)). Furthermore, changes in lens movement parameters, such as frequency, Q -factor, damping ratio, and D_{\max} , following the WDT indicate a substantial effect on ocular physiology.

The wobbling pattern of the crystalline lens exhibits significant individual variability, as illustrated in Figure 9, indicating that this movement is not uniform across subjects. This inconsistency suggests that the factors governing lens movement and adaptation are complex and may not be solely dependent on the presence of a wobbling pattern. Drawing on previous work (Chapter 3) ([Dahaghin et al., 2024a](#)), the study highlights the importance of zonular fibers in this phenomenon, noting that their mechanical properties vary between individuals ([Boszczyk et al., 2023](#)), potentially contributing to the observed differences.

A wide range of estimated Q -factors, reflects the complex interplay of lens dynamics and individual physiological responses. Some individuals show increase, while others exhibit a decrease, indicating varied responses to stimuli. A notable increase in damping ratios suggests a diminished persistence of lens movement across most subjects, and a reduction in D_{\max} implies a decrease in the range of lens movement, potentially affecting visual flexibility and accommodation ([He et al., 2012](#)). This underscores the critical need for adequate lens mobility for optimal vision. Research into minimizing the impact of IOP on lens dynamics, including strategies to enhance lens control and stability, is imperative ([Leydolt et al., 2008](#)). Optomechanical modeling of the eye under escalating IOP levels mirrors experimental findings, showing increased damping factors that indicate greater stability at higher pressures. Conversely, D_{\max} and Q -factor parameters decrease, suggesting reduced lens oscillations that could affect visual function.

6.6 Conclusion

The current chapter illuminates the impact of IOP on the dynamic behavior of the crystalline lens, highlighting the necessity to account for mechanical variations during clinical assessments. The alignment of experimental outcomes with simulation data confirms the efficacy of the simulated model in investigating lens dynamics and evaluating IOP's effects. This study opens avenues for developing advanced IOP measurement techniques, potentially through optical Purkinje imaging systems that could estimate IOP by observing lens oscillations. Unlike traditional methods such as air puffs, which may be uncomfortable and give the IOP estimates measured through the corneal tissue, the non-invasive Purkinje imaging system could improve patient comfort and measurement precision.

Chapter 7

Overall Conclusions

7.1 Conclusions

Ocular biomechanics has experienced significant growth in recent years, thanks to increasing support for interdisciplinary research. A single biomechanics project in this field can encompass various aspects of science. Ocular biomechanics at its core, it seeks to unravel the intricate interplay between the mechanical interaction of ocular tissues and their optical responses. From studying the crystalline lens overshooting to elucidating the impact of mechanical properties, each facet contributes to a comprehensive framework for analyzing ocular biomechanics. By modeling an *ex vivo* porcine eye, the study indicates a close match between modeling and experimental data, suggesting that it can effectively simulate porcine eyes *ex vivo*, reducing the need for multiple experiments.

Notably, this research represents the first numerical approach to describe and quantify the dynamics of the crystalline lens wobbling phenomenon. To the best of our knowledge, no prior studies have successfully modeled this effect with such precision. This breakthrough was made possible through the accurate and reliable modeling of the eye globe and the biomechanical parameters of its anatomical structures. By using finite element (FE) modeling, both *ex vivo* and *in vivo* experiments were successfully reconstructed, further validating the effectiveness of this approach.

An emerging trend in ocular biomechanics is the shift towards personalized medicine. Using geometrical and mechanical data, researchers can customize treatment strategies for individual patients, optimize outcomes, and minimize risks. Highlighting the importance of tissue biomechanics in the sclera, cornea, muscle, lens, and especially zonules, the study underscores the critical role of these factors in ocular dynamics. It emphasizes the pivotal role of zonules Young's modulus and Poisson's ratio in modeling lens overshooting.

The motivations driving studies in ocular biomechanics are diverse given the large number of people affected by ocular diseases, ranging from simple refractive errors to complex eye conditions. The advancement of technology has been instrumental in driving progress within the field of ocular biomechanics. From sophisticated tonometry modalities such as the Goldmann tonometer to cutting-edge non-contact (or air-puff) tonometers, researchers have an unparalleled collection of tools at their disposal to explore the intricacies of ocular mechanics. As an entirely novel finding, this research sheds light on how lenses react to changes in intraocular pressure, crucial for conditions such as glaucoma. The outcomes suggest potential applications in diagnostic tools and personalized treatments,

including non-invasive methods like the Purkinje imaging system for IOP estimation. In conclusion, the subject of crystalline lens overshooting is a rapidly developing field that holds promise for advancing our understanding of the ocular system.

7.2 Future Research

Subsequent suggestions for future studies are offered taking into account the limitations identified and the results obtained from the present research project:

1. Given the limitations of the study, such as the number of measured subjects and simplified models, it is suggested to incorporate *in vivo* data and consider other biomechanical factors for a complete understanding of the dynamics of the crystalline lens.
2. Performing measurements on a group of voluntary subjects, across a wide age and IOP range.
3. Utilizing a model that provide deeper insights into ocular responses to mechanical influences, including the exploration of non-linear materials and processes affecting eye health, such as fluid dynamics in the trabecular meshwork.

Bibliography

- ALLISON, K., PATEL, D. & ALABI, O. 2020. Epidemiology of glaucoma: the past, present, and predictions for the future. *Cureus*, 12.
- ANAND-APTE, B. & HOLLYFIELD, J. 2010. Developmental Anatomy of the Retinal and Choroidal Vasculature. *Encyclopedia of the Eye*, 9-15.
- ANGAYARKANNI, N., CORAL, K., BHARATHI DEVI, S. R. & SAIJYOTHI, A. V. 2016. The biochemistry of the eye. *Pharmacology of Ocular Therapeutics*, 83-157.
- ATCHISON, D. A. & THIBOS, L. N. 2016. Optical models of the human eye. *Clinical and Experimental Optometry*, 99, 99-106.
- AYYALASOMAYAJULA, A., PARK, R. I., SIMON, B. R. & VANDE GEEST, J. P. 2016. A porohyperelastic finite element model of the eye: the influence of stiffness and permeability on intraocular pressure and optic nerve head biomechanics. *Computer methods in biomechanics and biomedical engineering*, 19, 591-602.
- BARTHOLOMEW, R. 1970. Phakodonesis. A sign of incipient lens displacement. *The British Journal of Ophthalmology*, 54, 663.
- BEERS, A. & VAN DER HEIJDE, G. 1996. Age-related changes in the accommodation mechanism. *Optometry and vision science*, 73, 235-242.
- BENGTSSON, B., LESKE, M. C., HYMAN, L., HEIJL, A. & GROUP, E. M. G. T. 2007. Fluctuation of intraocular pressure and glaucoma progression in the early manifest glaucoma trial. *Ophthalmology*, 114, 205-209.
- BETTS, J. G., YOUNG, K. A., WISE, J. A., JOHNSON, E., POE, B., KRUSE, D. H., KOROL, O., JOHNSON, J. E., WOMBLE, M. & DESAIX, P. 2013. *Anatomy and Physiology*, Houston, Texas, OpenStax.
- BOCSKAI, Z. & BOJTÁR, I. 2013. Biomechanical modelling of the accommodation problem of human eye. *periodica polytechnica Civil Engineering*, 57, 3-9.
- BODDU, S. H., MENEES, A. L., RAY, A. & MITRA, A. K. 2013. A brief overview of ocular anatomy and physiology. *Treatise on Ocular Drug Delivery*, 1.
- BOSZCZYK, A., DĘBOWY, F., JÓŹWIK, A., DAHAGHIN, A. & SIEDLECKI, D. 2023. Complexity of crystalline lens wobbling investigated by means of combined mechanical and optical simulations. *Biomedical Optics Express*, 14, 2465-2477.
- BOURGE, J.-L., ROBERT, A., ROBERT, L. & RENARD, G. 2007. Zonular fibers, multimolecular composition as related to function (elasticity) and pathology. *Pathologie Biologie*, 55, 347-359.

- BROWN, N. 1973. The change in shape and internal form of the lens of the eye on accommodation. *Experimental eye research*, 15, 441-459.
- BRUSINI, P., SALVETAT, M. L. & ZEPPIERI, M. 2021. How to measure intraocular pressure: an updated review of various tonometers. *Journal of clinical medicine*, 10, 3860.
- CABEZA-GIL, I., TAHSINI, V. & KLING, S. 2023. Viscoelastic properties of porcine lenses using optical coherence elastography and inverse finite element analysis. *Experimental eye research*, 233, 109558.
- CABEZA-GIL, I., GRASA, J. & CALVO, B. 2021. A validated finite element model to reproduce Helmholtz's theory of accommodation: a powerful tool to investigate presbyopia. *Ophthalmic and Physiological Optics*, 41, 1241-1253.
- CHEN, X. & STOJANOVIC, A. 2017. *Corneal optical regularization and biomechanical stabilization in keratoconus and irregular astigmatism by use of topography-guided custom ablation and corneal cross-linking*. Ph.D. Thesis, University of Oslo.
- CHIEN, C.-H. M., HUANG, T. & SCHACHAR, R. A. 2006. Analysis of human crystalline lens accommodation. *Journal of biomechanics*, 39, 672-680.
- COLDRICK, B. 2013. *Modelling the human accommodation system using finite element analysis*. Ph.D. Thesis, Aston University.
- COSTAGLIOLA, C., DELL'OMO, R., AGNIFILI, L., BARTOLLINO, S., FEA, A. M., UVA, M. G., ZEPPA, L. & MASTROPASQUA, L. 2020. How many aqueous humor outflow pathways are there? *Survey of Ophthalmology*, 65, 144-170.
- COURTNEY, T. H. 2005. *Mechanical behavior of materials*, Waveland Press.
- D'OMBRAIN, A. 1936. TREMULOUS LENS. *The British Journal of Ophthalmology*, 20, 22.
- DA SILVA, F. & LIRA, M. 2022. Intraocular pressure measurement: A review. *Survey of Ophthalmology*, 67, 1319-1331.
- DAHAGHIN, A., SALIMIBANI, M., BOSZCZYK, A., JÓZWIK, A., SKROK, M., GRASA, J. & SIEDLECKI, D. 2024a. Investigation of crystalline lens overshooting: ex vivo experiment and optomechanical simulation results. *Frontiers in Bioengineering and Biotechnology*, 12, 1348774.
- DAHAGHIN, A., SALIMIBANI, M., BOSZCZYK, A. & SIEDLECKI, D. 2024b. Effect of Tissue Parameters on the Dynamics of Crystalline Lens Overshooting. *Investigative Ophthalmology & Visual Science*, 65, 5041-5041.

- DAI, P., ZHAO, Y., SHENG, H., LI, L., WU, J. & HAN, H. 2017. Simulating the effects of elevated intraocular pressure on ocular structures using a global finite element model of the human eye. *Journal of Mechanics in Medicine and Biology*, 17, 1750038.
- DAVID, G., PEDRIGI, R. M. & HUMPHREY, J. 2017. Accommodation of the human lens capsule using a finite element model based on nonlinear regionally anisotropic biomembranes. *Computer Methods in Biomechanics and Biomedical Engineering*, 20, 302-307.
- DOUGHTY, M. J. & ZAMAN, M. L. 2000. Human corneal thickness and its impact on intraocular pressure measures: a review and meta-analysis approach. *Survey of ophthalmology*, 44, 367-408.
- DOWNS, J. C., BURGOYNE, C. F., SEIGFREID, W. P., REYNAUD, J. F., STROUTHIDIS, N. G. & SALLEE, V. 2011. 24-hour IOP telemetry in the nonhuman primate: implant system performance and initial characterization of IOP at multiple timescales. *Investigative ophthalmology & visual science*, 52, 7365-7375.
- ELSHEIKH, A., WANG, D., BROWN, M., RAMA, P., CAMPANELLI, M. & PYE, D. 2007. Assessment of corneal biomechanical properties and their variation with age. *Current eye research*, 32, 11-19.
- EPPIG, T., GILLNER, M., ZORIC, K., JÄGER, J., LÖFFLER, A. & LANGENBUCHER, A. 2013. Biomechanical eye model and measurement setup for investigating accommodating intraocular lenses. *Zeitschrift für Medizinische Physik*, 23, 144-152.
- ETMINAN, A., SALIMIBANI, M., DAHAGHIN, A., HAGHPANAHI, M. & MALEKI, A. 2023. FEM thermal assessment of a 3-D irregular tumor with capillaries in magnetic nanoparticle hyperthermia via dissimilar injection points. *Computers in Biology and Medicine*, 157, 106771.
- FISHER, R. 1977. The force of contraction of the human ciliary muscle during accommodation. *The Journal of physiology*, 270, 51-74.
- GAMBRA, E., ORTIZ, S., PEREZ-MERINO, P., GORA, M., WOJTKOWSKI, M. & MARCOS, S. 2013. Static and dynamic crystalline lens accommodation evaluated using quantitative 3-D OCT. *Biomedical optics express*, 4, 1595-1609.
- GENEST, R. 2010. *Effect of intraocular pressure on chick eye geometry, finite element modeling, and myopia*. Master Thesis, University of Waterloo.
- HE, L., WENDT, M. & GLASSER, A. 2012. Manipulation of intraocular pressure for studying the effects on accommodation. *Experimental eye research*, 102, 76-84.

- HEYS, K. R., CRAM, S. L. & TRUSCOTT, R. J. 2004. Massive increase in the stiffness of the human lens nucleus with age: the basis for presbyopia? *Molecular Vision* 2004, 10:956-63.
- HUEBNER, K. H., DEWHIRST, D. L., SMITH, D. E. & BYROM, T. G. 2001. *The finite element method for engineers*, John Wiley & Sons.
- ISSARTI, I., KOPPEN, C. & ROZEMA, J. J. 2021. Influence of the eye globe design on biomechanical analysis. *Computers in biology and medicine*, 135, 104612.
- JACOBI, K. W. & JAGGER, W. S. 1981. Physical forces involved in pseudophacodonesis and iridodonesis. *Albrecht von Graefes Archiv für klinische und experimentelle Ophthalmologie*, 216, 49-53.
- JANULEVICIENE, I., KUZMIENE, L. & SLIESORAITYTE, I. 2006. Comparison of intraocular pressure fluctuations measured by Goldmann applanation tonometer and pulsatile ocular blood flow analyser. *International Journal of Biomedical Science: IJBS*, 2, 428.
- JIN, Y., WANG, X., ZHANG, L., JONAS, J. B., AUNG, T., SCHMETTERER, L. & GIRARD, M. J. 2018. Modeling the origin of the ocular pulse and its impact on the optic nerve head. *Investigative ophthalmology & visual science*, 59, 3997-4010.
- JOSELEVITCH, C. 2008. Human retinal circuitry and physiology. *Psychology & Neuroscience*, 1, 141.
- KAUFMAN, P. L. 2005. Changes in aqueous humor dynamics with age and glaucoma. *Progress in retinal and eye research*, 24, 612-637.
- KLEINBERG, T. T., TZEKOV, R. T., STEIN, L., RAVI, N. & KAUSHAL, S. 2011. Vitreous substitutes: a comprehensive review. *Survey of ophthalmology*, 56, 300-323.
- KNUDSON, D. V. & KNUDSON, D. 2007. *Fundamentals of biomechanics*, Springer.
- KORETZ, J. F. & HANDELMAN, G. H. 1988. How the human eye focuses. *Scientific American*, 259, 92-99.
- KORI, S. 2018. Time since death from rigor mortis: forensic prospective. *Journal of Forensic Sciences & Criminal Investigation*, 9, 555771.
- LEYDOLT, C., FINDL, O. & DREXLER, W. 2008. Effects of change in intraocular pressure on axial eye length and lens position. *Eye*, 22, 657-661.
- LJUBIMOVA, D. 2009. *Biomechanics of the human eye and intraocular pressure measurements*. Doctoral Thesis, KTH.
- LUND, E. 1994. *Finite element based design sensitivity analysis and optimization*. 107 Ph.D. Dissertation.

- MACHIELE, R., MOTLAGH, M. & PATEL, B. C. 2018. Intraocular pressure.
- MAHIL, A.-D. 2018. *Optical Coherence Tomography of the Human Crystalline Lens and Its Application to the Structural Assessment of Cataract in the Down Syndrome Eye*. Doctoral Thesis, Ulster University.
- MAKLAD, O. M. Y. 2019. *Influence of fluid-structure interaction on human eye biomechanics under air puff non-contact tonometry*. Ph.D. Thesis, The University of Liverpool.
- MARKOV, P. P. 2020. *Cellular and extracellular aspects of posterior eye microstructure and biomechanics*. Ph.D. Thesis, Cardiff University.
- MARTIN, H., BAHLKE, U., GUTHOFF, R., RHEINSCHMITT, L. & SCHMITZ, K. Determination of inertia forces at an intraocular lens implant during saccades. World Congress on Medical Physics and Biomedical Engineering, September 7-12, 2009, Munich, Germany: Vol. 25/11 Biomedical Engineering for Audiology, Ophthalmology, Emergency & Dental Medicine, 2009. Springer, 100-103.
- MCBRIEN, N. A., JOBLING, A. I. & GENTLE, A. 2009. Biomechanics of the sclera in myopia: extracellular and cellular factors. *Optometry and vision science*, 86, E23-E30.
- MEEK, K. M. & KNUPP, C. 2015. Corneal structure and transparency. *Progress in retinal and eye research*, 49, 1-16.
- MENDUNI, F., DAVIES, L. N., MADRID-COSTA, D., FRATINI, A. & WOLFFSOHN, J. S. 2018. Characterisation of the porcine eyeball as an in-vitro model for dry eye. *Contact Lens and Anterior Eye*, 41, 13-17.
- MOAZED, K. T. & MOAZED, K. T. 2020. Iris histology. *The Iris: Understanding the Essentials*, 31-50.
- MOGHADDAM, H. A. & MERTINY, P. 2019. Stochastic finite element analysis framework for modelling mechanical properties of particulate modified polymer composites. *Materials*, 12.
- NAPIERALSKI, P. & RYNKIEWICZ, F. 2019. Modeling human pupil dilation to decouple the pupillary light reflex. *Open Physics*, 17, 458-467.
- NAVARRO, R., SANTAMARIA, J. & BESCÓS, J. 1985. Accommodation-dependent model of the human eye with aspherics. *JOSA A*, 2, 1273-1280.
- NICOGUARO. 2020. *Typical stress vs. strain diagram for a ductile material (e.g. steel)* This file is licensed under the Creative Commons Attribution 4.0 International license (Canonical URL <https://creativecommons.org/licenses/by/4.0/>) [Online]. Wikipedia. Available: https://commons.wikimedia.org/wiki/File:Stress_strain_ductile.svg [Accessed 27 October 2024].

- NYSTRÖM, M., ANDERSSON, R., MAGNUSSON, M., PANSELL, T. & HOOGE, I. 2015. The influence of crystalline lens accommodation on post-saccadic oscillations in pupil-based eye trackers. *Vision research*, 107, 1-14.
- OFRI, R. 2013. Optics and physiology of vision. *Veterinary ophthalmology*, 1, 208-269.
- OKEREKE, M., KEATES, S., OKEREKE, M. & KEATES, S. 2018. Finite element mesh generation. *Finite Element Applications: A Practical Guide to the FEM Process*, 165-186.
- OSMERS, J., KAISER, N., SORG, M. & FISCHER, A. 2021. Adaptive finite element eye model for the compensation of biometric influences on acoustic tonometry. *Computer Methods and Programs in Biomedicine*, 200, 105930.
- ÖZKAYA, N., LEGER, D., GOLDSHEYDER, D. & NORDIN, M. 2017. *Fundamentals of Biomechanics*, Cham, Springer
- PAN, Y., LIU, Z. & ZHANG, H. 2023. Research progress of lens zonules. *Advances in Ophthalmology Practice and Research*, 3, 80-85.
- PIERSCIONEK, B. K. 1993. In vitro alteration of human lens curvatures by radial stretching. *Experimental Eye Research*, 57, 629-635.
- PIÑERO, D. P. & ALCÓN, N. 2015. Corneal biomechanics: a review. *Clinical and Experimental Optometry*, 98, 107-116.
- POWER, E. D. 2001. *A nonlinear finite element model of the human eye to investigate ocular injuries from night vision goggles*. Master Thesis, Virginia Tech.
- PRZEŹDZIECKA-DOŁYK, J., WAŁEK, E., JÓŹWIK, A., HELEMEJKO, I., ASEJCZYK-WIDLICKA, M. & MISIUK-HOJŁO, M. 2021. Short-time changes of intraocular pressure and biomechanics of the anterior segment of the eye during water drinking test in patients with XEN GelStent. *Journal of Clinical Medicine*, 11, 175.
- REDAELLI, E., GRASA, J., CALVO, B., RODRIGUEZ MATAS, J. F. & LURAGHI, G. 2022. A detailed methodology to model the Non Contact Tonometry: a Fluid Structure Interaction study. *Frontiers in Bioengineering and Biotechnology*, 10, 981665.
- REGAL, S., TROUGHTON, J., DJENIZIAN, T. & RAMUZ, M. 2021. Biomimetic models of the human eye, and their applications. *Nanotechnology*, 32, 302001.
- REPETTO, R. & TWEEDY, J. H. 2018. 22. Biomechanics of the vitreous humor. *Biomechanics of the Eye*, 323.
- RIDLEY, F. 1930. The intraocular pressure and drainage of the aqueous humour. *British journal of experimental pathology*, 11, 217.

- ROSZKOWSKA, A. M. & TORRISI, L. Intraocular lens employed for cataract surgery. *Journal of Physics: Conference Series*, 2014. IOP Publishing, 012014.
- SALIMI, S., SIMON PARK, S. & FREIHEIT, T. 2011. Dynamic response of intraocular pressure and biomechanical effects of the eye considering fluid-structure interaction. *Journal of Biomechanical Engineering*, 133(9): 091009.
- SANCHEZ, I., MARTIN, R., USSA, F. & FERNANDEZ-BUENO, I. 2011. The parameters of the porcine eyeball. *Graefe's Archive for Clinical and Experimental Ophthalmology*, 249, 475-482.
- SCHMIDL, D., GARHOFER, G. & SCHMETTERER, L. 2011. The complex interaction between ocular perfusion pressure and ocular blood flow—relevance for glaucoma. *Experimental eye research*, 93, 141-155.
- SERBECIC, N., BEUTELSPACHER, S., MARKOVIC, L., ROY, A. S. & SHETTY, R. 2020. Repeatability and reproducibility of corneal biomechanical parameters derived from Corvis ST. *European Journal of Ophthalmology*, 30, 1287-1294.
- SINGH, D., FIROUZBAKHS, K. & AHMADIAN, M. T. 2017. Human intraocular thermal field in action with different boundary conditions considering aqueous humor and vitreous humor fluid flow. *International Journal of Mechanical and Mechatronics Engineering*, 11, 717-725.
- SMITH, G., PIERSCIONEK, B. K. & ATCHISON, D. A. 1991. The optical modelling of the human lens. *Ophthalmic and Physiological Optics*, 11, 359-369.
- STREETEN, B. W. 1982. The nature of the ocular zonule. *Transactions of the American Ophthalmological Society*, 80, 823.
- SUSANNA, R., VESSANI, R., SAKATA, L., ZACARIAS, L. & HATANAKA, M. 2005. The relation between intraocular pressure peak in the water drinking test and visual field progression in glaucoma. *British journal of ophthalmology*, 89, 1298-1301.
- TABERNERO, J. & ARTAL, P. 2014. Lens oscillations in the human eye. Implications for post-saccadic suppression of vision. *PloS one*, 9, e95764.
- TABERNERO, J., BENITO, A., NOURRIT, V. & ARTAL, P. 2006. Instrument for measuring the misalignments of ocular surfaces. *Optics Express*, 14, 10945-10956.
- TAMM, E. R., BRAUNGER, B. M. & FUCHSHOFER, R. 2015. Intraocular pressure and the mechanisms involved in resistance of the aqueous humor flow in the trabecular meshwork outflow pathways. *Progress in molecular biology and translational science*, 134, 301-314.

- TRUSCOTT, R. J. 2005. Age-related nuclear cataract—oxidation is the key. *Experimental eye research*, 80, 709-725.
- URS, R., HO, A., MANNS, F. & PAREL, J.-M. 2010. Age-dependent Fourier model of the shape of the isolated ex vivo human crystalline lens. *Vision research*, 50, 1041-1047.
- VAN ALPHEN, G. & GRAEBEL, W. P. 1991. Elasticity of tissues involved in accommodation. *Vision Research*, 31, 1417-1438.
- WANG, K. & PIERSCIONEK, B. K. 2019. Biomechanics of the human lens and accommodative system: Functional relevance to physiological states. *Progress in retinal and eye research*, 71, 114-131.
- WANG, K., VENETSANOS, D. T., WANG, J., AUGOUSTI, A. T. & PIERSCIONEK, B. K. 2017. The importance of parameter choice in modelling dynamics of the eye lens. *Scientific Reports*, 7, 16688.
- WATSON, P. G. & YOUNG, R. D. 2004. Scleral structure, organisation and disease. A review. *Experimental eye research*, 78, 609-623.
- WATSON, R., GRAY, W., SPONSEL, W. E., LUND, B. J., GLICKMAN, R. D., GROTH, S. L. & REILLY, M. A. 2015. Simulations of porcine eye exposure to primary blast insult. *Translational vision science & technology*, 4, 8-8.
- WHITELEY, J. 2014. *Finite element methods, A Practical Guide*, Cham, Springer.
- WONG, K.-H., KOOPMANS, S. A., TERWEE, T. & KOOIJMAN, A. C. 2007. Changes in spherical aberration after lens refilling with a silicone oil. *Investigative ophthalmology & visual science*, 48, 1261-1267.
- ZAPATA-DÍAZ, J. F., RADHAKRISHNAN, H., CHARMAN, W. N. & LÓPEZ-GIL, N. 2019. Accommodation and age-dependent eye model based on in vivo measurements. *Journal of optometry*, 12, 3-13.
- ZHALGAS, A., KO, M. W. & KIM, J. R. Determination of corneal nonlinear viscoelastic biomechanical properties using Corvis ST. 2019 IEEE 19th International Conference on Bioinformatics and Bioengineering (BIBE), 2019. IEEE, 634-637.
- ZHANG, Y., RASKU, J. & JUHOLA, M. 2012. Biometric verification of subjects using saccade eye movements. *International Journal of Biometrics*, 4, 317-337.
- ZHOU, B., SIT, A. J. & ZHANG, X. 2017. Noninvasive measurement of wave speed of porcine cornea in ex vivo porcine eyes for various intraocular pressures. *Ultrasonics*, 81, 86-92.

ZOUACHE, M. A., EAMES, I. & SAMSUDIN, A. 2016. Allometry and scaling of the intraocular pressure and aqueous humour flow rate in vertebrate eyes. *PLoS One*, 11, e0151490

List of Figures

Figure 1. The anatomy of the eye.	6
Figure 2. Purkinje images PI-PIV, PIII is indistinguishable.	13
Figure 3. Tracking PI (corneal reflection) and PIV (lens reflection) positions for two different subjects. The black circles represent the stable PI positions, while the green circles track the PIV positions, which exhibit post-saccadic oscillations.	14
Figure 4. Wobbling data for two different subjects depending on their orientation.	14
Figure 5. Schematic of the FEM steps for modeling and analysis.	17
Figure 6. Element dimensions for (a) 1D, (b) 2D and (c) 3D elements.	17
Figure 7. Typical stress–strain curve.	18
Figure 8. Overshooting effect observed in the examined eye <i>ex vivo</i>	24
Figure 9. Wobbling patterns for six different subject (physiological IOP).	25
Figure 10. Comparison of wobbling patterns for six different subjects, illustrating both physiological IOP and post-WDT measurements.	25
Figure 11. (A) Dimensions of the finite element model. (B) Mesh arrangement.	29
Figure 12. Parametrization of the overshooting trajectory.	31
Figure 13. Overshooting magnitude in the experimental and simulation results.	32
Figure 14. Damping function.	33
Figure 15. Steps in performing the sensitivity analysis.	39
Figure 16. Quantified parameters of the crystalline lens apex displacement.	41
Figure 17. Percentage share of variations in D_{max} for different Young's modulus used in the model components.	42
Figure 18. Percentage share of variations in t_{peak} for different Young's modulus used in the model components.	42
Figure 19. Percentage share of variations in $t_{balance}$ for different Young's modulus used in the model components.	43
Figure 20. Displacement magnitude in the lens under varying conditions of Young's modulus in different parts of the eye.	45
Figure 21. Displacement magnitude in the lens under varying conditions of Poisson's Ratio in different structures of the eye.	46
Figure 22. Percentage share of variations in t_{peak} , $t_{balance}$ and D_{max} for different Poisson's ratio values used for zonular fiber.	47

Figure 23. Illustration of decentration and tilt of the crystalline lens being induced by rotation motion of the whole eye globe.	54
Figure 24. Time evolution of apex position of the crystalline lens during overshooting....	55
Figure 25. The trend of observed changes in $t_{balance}$, t_{peak} and D_{max} , with increasing IOP levels.....	58
Figure 26. Analyzing trends based on the percentage change in lens displacement patterns across various levels of intraocular pressure.	59
Figure 27. Steps involved in the study and simulation process. The diagram outlines the key stages and their interconnections, providing a visual guide to the overall workflow.	64
Figure 28. Geometry of the model containing the main and the most influential elements in eye biomechanics: lens, capsular bag, vitreous body, zonular fibers, cornea, sclera, aqueous humour and ciliary muscle.	65
Figure 29. Analysed parameters for WDT results.....	69
Figure 30. Simulation pattern for all IOP levels.....	69
Figure 31. Analysed parameters for simulation results.	70

List of Tables

Table 1. Eye model parameters in which age and accommodation stimulus are included as variables.....	22
Table 2. Material properties of the porcine eye.....	30
Table 3. Detailed data related to the errors.....	32
Table 4. Damping data.....	33
Table 5. Material properties of the porcine eye (The baseline values are highlighted in grey).	40
Table 6. Different Young's modulus values and corresponding: D_{max} , t_{peak} , and $t_{balance}$ for various tissues (sclera, cornea, muscle, lens, and zonule). Each row involves the alteration of the Young modulus of the specific tissue, while the standard value for the other tissues remains unaltered.....	44
Table 7. Different Poisson's ratio values for the zonular fibers and its corresponding effect on D_{max} , t_{peak} , and $t_{balance}$	46
Table 8. The maximum velocity and acceleration data of the apex position of the crystalline lens during overshooting for all IOP levels.	56
Table 9. Overshooting parameters for the six IOP levels and their relative variation with respect to the initial level of 15 mmHg.	57
Table 10. Summary of geometrical parameters.....	64
Table 11. Mechanical Properties Assigned to Ocular Tissues.	65
Table 12. Summary of optical parameters.....	66
Table 13. Wobbling data.	68
Table 14. Simulation data for all IOP levels.	70